DEFORMATION CHARACTERISTICS OF SAND SUBJECTED TO ANISOTROPIC CYCLIC, DYNAMIC LOADING

THESIS FOR THE DEGREE OF Ph. D.
MICHIGAN STATE UNIVERSITY

DAVID HAROLD TIMMERMAN
1969

This is to certify that the

thesis entitled

DEFORMATION CHARACTERISTICS OF
SAND SUBJECTED TO ANISOTROPIC
CYCLIC, DYNAMIC LOADING

presented by

David H. Timmerman

has been accepted towards fulfillment
of the requirements for

Ph.D. degree in Civil Engineering

R. K. Wilson
Major professor

Date February 20, 1969

ABSTRACT

DEFORMATION CHARACTERISTICS OF SAND
SUBJECTED TO ANISOTROPIC
CYCLIC, DYNAMIC LOADING

By

David H. Timmerman

The magnitude of irrecoverable foundation settlement that can be expected to occur progressively with each cycle of a vibratory loading cannot be adequately determined by existing theories in most cases. This study was undertaken, therefore, in an attempt to develop a better qualitative understanding of dynamic soil deformation characteristics and to determine basic relationships which could be used to express the soil deformation in a quantitative manner.

In order to obtain stress-deformation relationships in the laboratory which could be used for settlement computations, it was necessary to reproduce the in situ stress conditions in the experiments. This was accomplished with a modified triaxial cell and a specially designed loading mechanism to apply cyclic loadings to the specimens. With this apparatus, specimens of air-dried Ottawa sand were first loaded statically to a specified anisotropic stress state to represent the

in situ static stress state existing under a foundation. A sinusoidal loading was then superimposed upon the existing static stress state in one of two ways. Either a cyclic axial stress or a cyclic confining pressure was applied. The frequency of the cyclic loadings varied from 0.1 to 25.0 cps. The applied loadings and the resulting axial and radial deformations were measured electronically.

The variables studied during the experimental investigation were the static principal stress ratio, R_s, i.e., the ratio of axial to radial stress, the maximum stress ratio, R_m, to which the specimen was subjected during the cyclic loading, the frequency of the cyclic loading, f, and the initial void ratio of the sand, e_o.

The axial strain resulting from 10,000 cycles of loading was considered as the dynamic strain under the given stress condition. For a sand with a given initial void ratio, e_o, this dynamic strain was correlated with a stress factor $F=R_m^3 R_D^{\frac{1}{2}}$, where $R_D=(R_m-R_s)/R_m$.

This dynamic strain was not unique for a given stress state, however. It was found to have two distinct possible magnitudes; a higher strain level and a lower strain level. The frequency of having a higher strain level increased as the void ratio, e_o, and the stress factor, F, increased.

Two significant stress levels, F_c, and F_f, were noted. The dynamic strains for loadings where F was smaller than F_c, were small. When F was greater than F_c, the resulting dynamic strains were proportionately much larger.

F_f denotes the stress level at which the sand specimen would fail under the dynamic loading. For loadings with F less than F_f, the resulting dynamic strains were of limited, well-defined magnitude. For loadings with F greater than F_f, the dynamic strains were much larger and of undefined magnitude. F_f was found to be a function of the magnitude of the cyclic stress as indicated by R_D.

The dynamic strains were found to be independent of the frequency of the load applications for frequencies between 2.5 and 25 cps; however, the strains were larger for slow repetitive loadings at 0.1 cps.

The volumetric strains were measured during the experimental investigation and were found to be a function of R_m and R_s. For tests with R_s below a certain value, R_v, the soil densified during the cyclic loading with the amount of densification increasing as R_m increased. For tests with R_s greater than R_v, the soil expanded during the cyclic loading. The expansion increased with increasing R_m.

DEFORMATION CHARACTERISTICS OF SAND SUBJECTED TO ANISOTROPIC CYCLIC, DYNAMIC LOADING

By
David H. Timmerman

A THESIS

Submitted to
Michigan State University
in partial fulfillment of the requirements
for the degree of

DOCTOR OF PHILOSOPHY

Department of Civil Engineering

1969

ACKNOWLEDGEMENTS

The author is grateful to his advisor, Dr. T.H. Wu, for the time, support, encouragement, and suggestions which he provided; to the Civil Engineering Department of Ohio State University for providing laboratory space and equipment necessary for the conduct of the investigation; to the men of the Civil Engineering machine shop for their invaluable assistance in designing and fabricating much of the equipment for the project; and to Michigan State University for the NDEA Fellowship which enabled the author to continue his education.

Special thanks go to his wife, Fay, for her encouragement and assistance in preparing this manuscript.

TABLE OF CONTENTS

LIST OF TABLES

LIST OF FIGURES

LIST OF APPENDICES

APPENDIX PAGE

CHAPTER I

INTRODUCTION

In recent years, considerable attention has been given to the field of soil dynamics and, in particular, to the problems relating to the soil-foundation response characteristics for various types of dynamic loadings. These dynamic loadings may be impulse loadings such as those caused by explosions, or vibratory loadings such as those produced by earthquakes, reciprocating engines, etc.

In particular, it is often important to determine the amount of irrecoverable settlement that can be expected to occur progressively with each cycle of vibratory loading.

Since the magnitude of such settlements resulting from vibratory loading cannot be adequately determined by existing theories in most cases, this study was undertaken in an attempt to develop a better qualitative understanding of dynamic soil deformation characteristics and to determine basic relationships which can be used to express the soil deformation behavior in a quantitative manner. With such information, it should be possible to analyze the general problem of foundation settlements under vibratory loads.

1.1 General Stress-Deformation Considerations

In order to determine the amount of settlement that would occur under a foundation subjected to a vibratory loading, it is first necessary to determine the static state of stress existing under the foundation plus the superimposed dynamic stress state due to the dynamic loading.

The static stress state can be estimated from existing stress distribution theories. Obtaining the dynamic stress state is another problem. However, as a result of research in this area, a reasonable estimate of the dynamic stress state can be made.

Assuming that the complete stress state existing under the foundation can be determined to a satisfactory degree of accuracy, knowledge of the dynamic stress-deformation relationships of the soil is required to estimate the settlement resulting from the dynamic loads.

Settlement under cyclic loading may be due to a combination of two factors. First, foundation settlement can result from densification of the soil in a zone under the foundation. Second, settlement can occur due to shearing deformations within the supporting soil mass. In addition to general shear deformations, shear surfaces could be developed or sections of the soil mass could be set in motion along developed shear surfaces.

Shear zones or zones of weakness could also be developed as a result of the shear and compression waves being transmitted through the supporting soil media from the vibrating foundation. Since these two types of waves to not propagate at the same velocity through the soil, there would be locations (at periodic distances from the foundation) where the two waves would be out of phase, i.e., the shearing stress (from the shear wave) would be at a maximum when the compressive stress (from the compression wave) would be at a minimum. If one or more of these locations falls within the zone of significant pressure under the foundation, the principal stress ratio at that location could lead to a local shear failure.

As a simplification, the foundation settlement can also be considered as the deformation of a block of soil that supports the foundation. (See Figure 1.) This deformation would include both volumetric strains (densification) and shear strains within the block.

This latter approach to the analysis of foundation settlement can be more easily compared with laboratory stress-deformation data, and is therefore taken in this study.

1.2 Stress State Beneath Loaded Footing

In order to obtain stress-deformation relationships in the laboratory which can be used for settlement computations, it is necessary to reproduce the in situ stress conditions in the experiments.

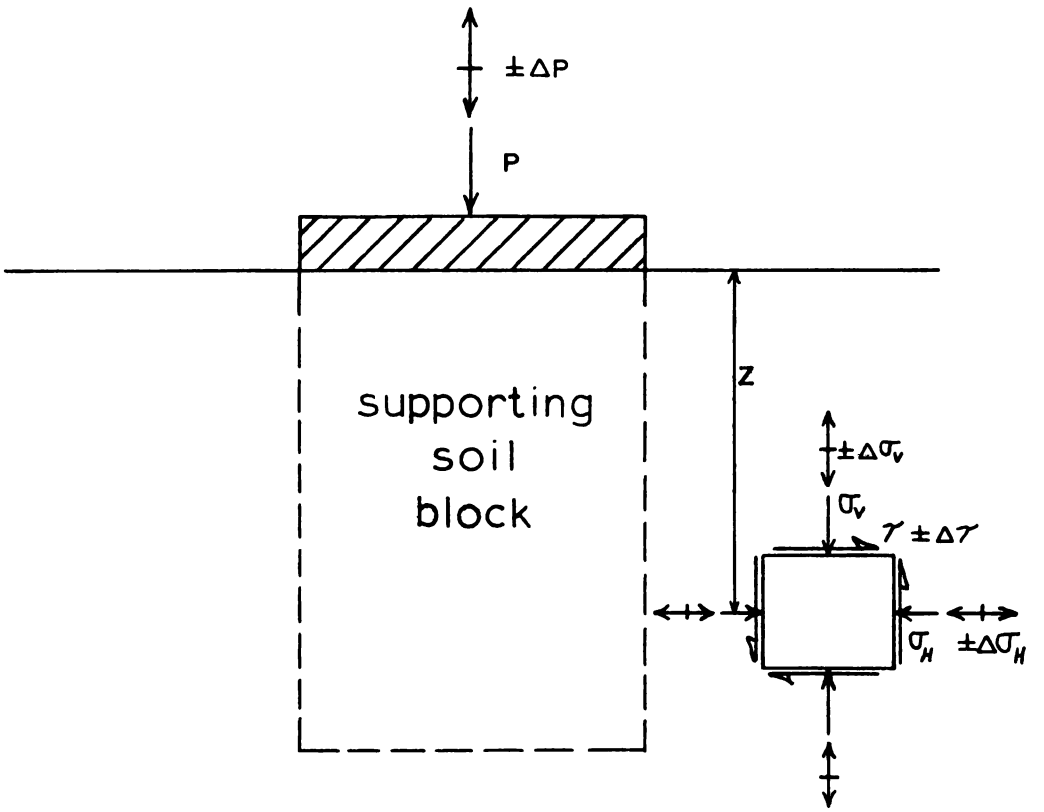

Fig. 1. --Stress state beneath loaded footing

The general stress state beneath a footing subjected to a vertical static and cyclic dynamic loading is shown in Figure 1. The vertical static load exerted by the footing is shown as P, and the cyclic load pulsating at a frequency, f, is shown as $\pm \Delta P$. At a distance, z, below the footing, an element of soil is subjected to a static stress plus a superimposed dynamic stress. The static stress state consists of a vertical stress, σ_V, a lateral stress, σ_H, and a shear stress, τ. These stresses are a combination of the at rest stress state of the soil plus the stress state from the static load on the foundation. The dynamic stress state consists of the cyclic vertical stress, $\pm\Delta\sigma_V$, the cyclic lateral stress, $\pm\Delta\sigma_H$, and the cyclic shear stress, $\pm\Delta\tau$. These stresses are the ones induced by the foundation under the action of the cyclic load, $\pm\Delta P$.

By restricting the investigation to the stress state existing under the center line of a vertically loaded circular footing, the stresses on the soil element shown in Figure 1 reduce to a radially symmetric state of stress with τ and $\Delta\tau$ being zero. Since this stress condition can be reproduced in a triaxial cell, the desired stress-deformation characteristics can be determined by this means in the laboratory.

1.3 Review of Literature

There has been considerable research performed in the area of soil dynamics. Much of this research has been concerned with general soil-foundation response characteristics

such as the work done by Alpan (1)*, Barkan (2), Lysmer (25) (26), Richart (30), Richart and Whitman (32), and Sung (39), and the stress distribution in the soil mass under dynamic loading such as the works of Bernhard (5) (7) (8) and Richart et.al (31).

Also having received considerable attention are the effects of dynamic loadings on soil properties. This line of research includes the investigations of dynamic shear strength and failure conditions by Johnson and Yoder (21), Linger (23), Mogami (27), Seed et.al (33) (35) (36) (37) (38), and Whitman and Healy (46), and the investigations of damping properties or energy absorption of the soil subjected to low amplitude vibrations by Hall and Richart (17), Hardin (18), Hardin and Black (19), and Weissmann and Hart (45).

Some information relating to stress-deformation characteristics has come from vibratory compaction studies. Early investigations along this line, such as those done by Bernhard (4) and Converse (11), were concerned primarily with determining what vibratory loading conditions at the soil surface would give maximum soil compaction. Although these works have shown the general effect of such variables as the magnitude of the applied loads, the area being loaded,

---

*Numbers in parentheses refer to the reference numbers of specific works listed in the bibliography.

and the cyclic frequency of the load repetitions on soil densification or deformation, they have not defined clearly the stress-deformation relationships of the soil.

Later vibratory compaction research by Gomes and Graves (16) indicated that the maximum compaction or densification occured at a given distance below the vibrating surface load with the relative density decreasing upward and downward from this location. In comparing this relative density vs. depth with the theoretical shear stress vs. depth, there appears to be a possible correlation between the magnitude of the shear stresses induced in the soil mass and the resulting relative density or deformation.

Since foundation settlement is related to changes in void ratio or porosity of the supporting soil, studies concerning the effects of dynamic loading upon the soil's void ratio are useful for studying foundation settlements. Barkan (2), Watanabe (44), and others have attempted to relate the acceleration of the imposed vibratory loading to the resulting void ratio attained by the soil. Each of these investigations has obtained a correlation between imposed acceleration and resulting void ratio. However, the various correlations are not in good agreement.

Bazant and Dvorak (3) suggested that besides acceleration, the frequency of the cyclic loading and the height and volume of the vibrating soil mass should also be considered as important factors in compaction.

As a result of the apparent discrepancies in the results of this type of research, the question was raised and investigated by Luscher (24) as to whether acceleration or some other variable such as stress should be considered the primary controlling variable. From this investigation (currently in progress) it appears that stress is probably the more important factor of the two, at least for accelerations less than 1 g.

In addition to laboratory research concerning soil behavior under cyclic loadings, there have been field and model investigations which measured the actual settlement of foundations subjected to dynamic loadings. Murphy (28) and Okamoto (29) measured the settlements of small, statically-loaded plates resting on sand when the entire system (soil and loaded plate) was subjected to a horizontal vibratory motion on a shaking table. Both investigators correlated the plate settlement with the acceleration of the shaking table.

Settlements have also been recorded for larger foundations. The Corps of Engineers (12) measured the settlements of 5 to 10 ft. diameter bases subjected to vertical static and cyclic loads.

All of the previously cited research contributes general information to the foundation settlement problem. However, the only studies concerning the irrecoverable deformation that can be expected to occur progressively with each cycle of vibratory loading are those by Luscher et.al.

(24), and Seed et.al. (36) (37) (38). Luscher's studies have not yet been completed and Seed's studies are limited to the condition of undrained loading of saturated sands.

CHAPTER II

EXPERIMENTAL INVESTIGATION

2.1 Equipment and Instrumentation

The most suitable type of test in general which allows the stresses to be controlled to the desired degree is the triaxial test. Therefore, it was decided to modify a standard triaxial cell so that the dynamic loading could also be applied. In order to have enough flexibility to study various aspects of the stress-deformation problem, a hydraulic loading system was devised so that the axial load and the cell pressure on the soil sample could be pulsed independently. The phase angle between the axial load and cell pressure could also be varied. This loading system is shown schematically in Figures 2 and 3. A Geonor triaxial cell for 1.4" diameter samples was used with additional openings tapped into the bottom to allow for a connecting line from the pulsating pressure cell, for electric outlets from the force transducer, LVDT, and thermocouple, and for the insertion of a pressure transducer.

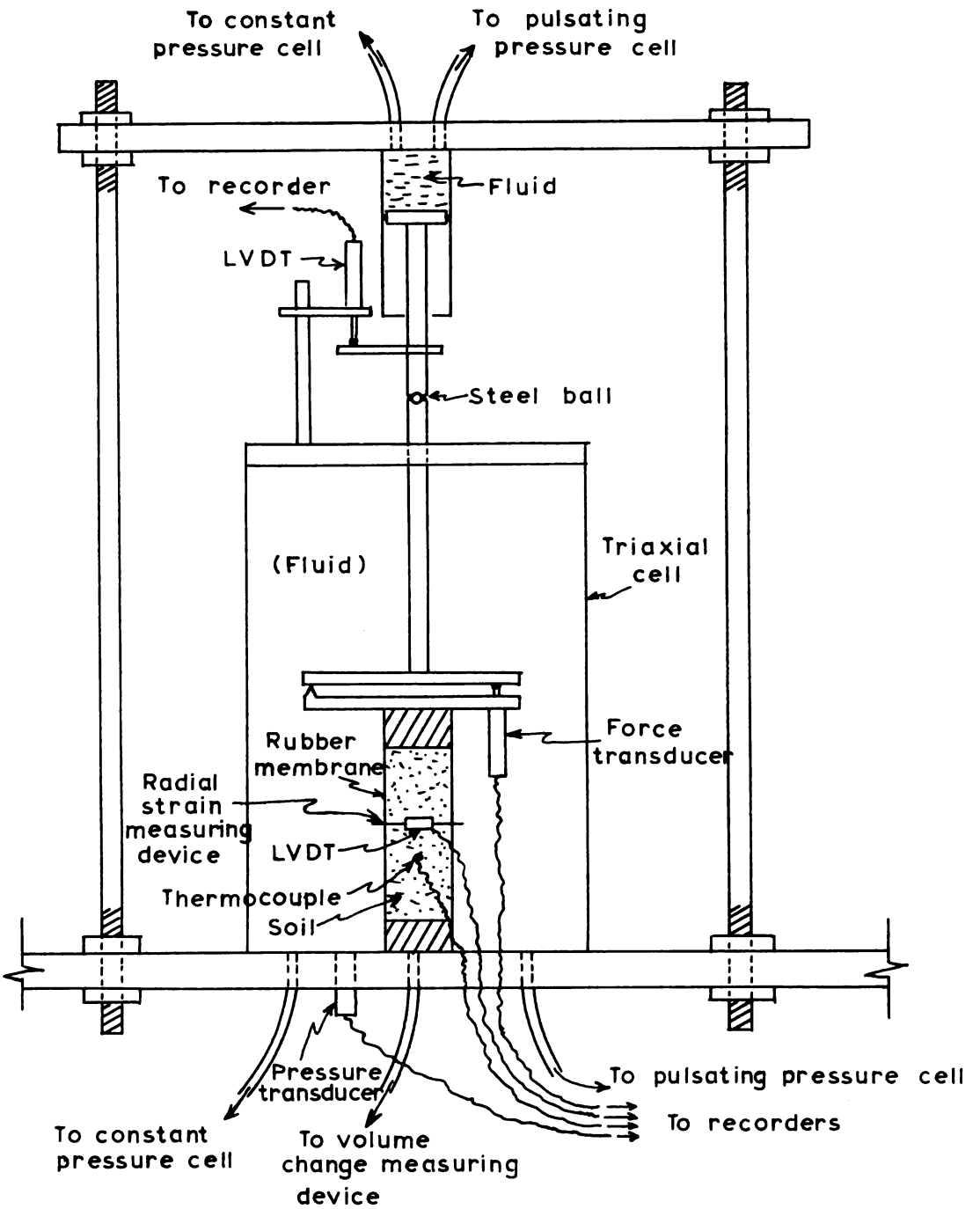

Fig. 2.-- Diagram of modified triaxial cell

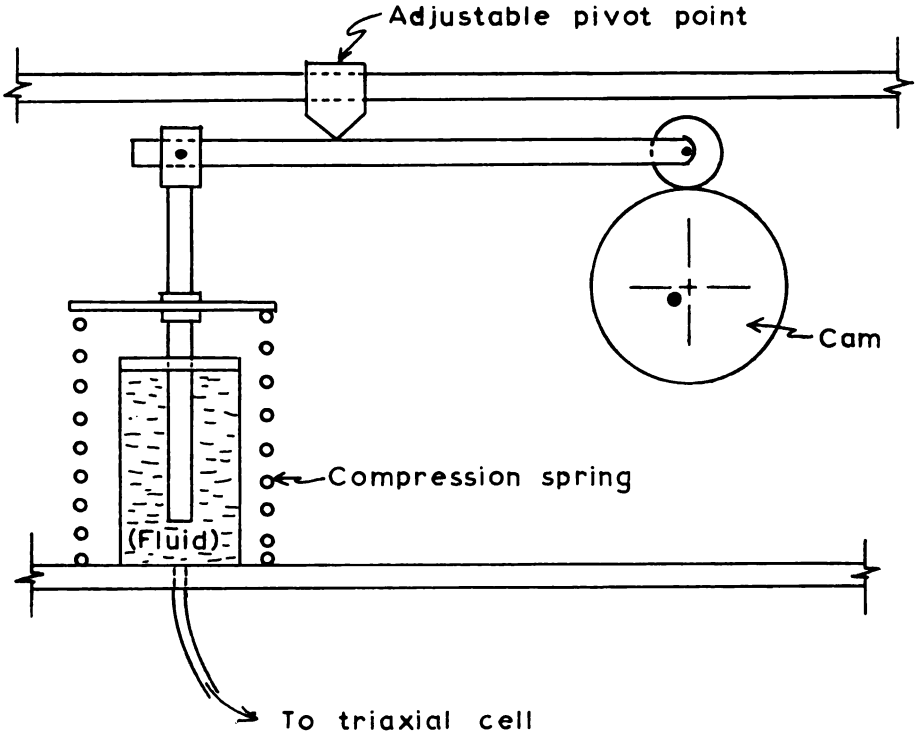

Fig. 3.--Diagram of pulsating pressure cell

The applied cell pressure was measured by means of a Dynisco Pressure Transducer (Model No. TCAPT25-1C) inserted into the base of the triaxial cell. A Dynisco Force Transducer (Model No. FT2-2C) was connected to the loading head (Figure 2) to measure the axial load on the sample. The force transducer was put inside the triaxial cell to measure the axial load at the top of the sample so that any friction between the piston and the bushing would not affect the load readings.

The lateral deformation of the sample was measured by means of the device shown in Figure 4. A Sanborn Linearsyn Differential Transformer (Model No. 595DT-100) was used. The axial deformation was measured with a Daytronic LVDT (Model No. 103C-200) mounted on the top of the cell as shown in Figure 2. The Electronic components and leads inside the triaxial cell were coated with silicon rubber for waterproofing.

The transducers that measure the axial load and the cell pressure were connected to a Tektronix Dual-Beam Oscilloscope (Type RM-565) equipped with two Tektronix Carrier Amplifiers (Type 3C66). This allowed the magnitude and frequency of the loads, and the phase angle between the two loads to be monitored continually. Any variations in the input loading could be noted and the necessary adjustments of the loading system could be made.

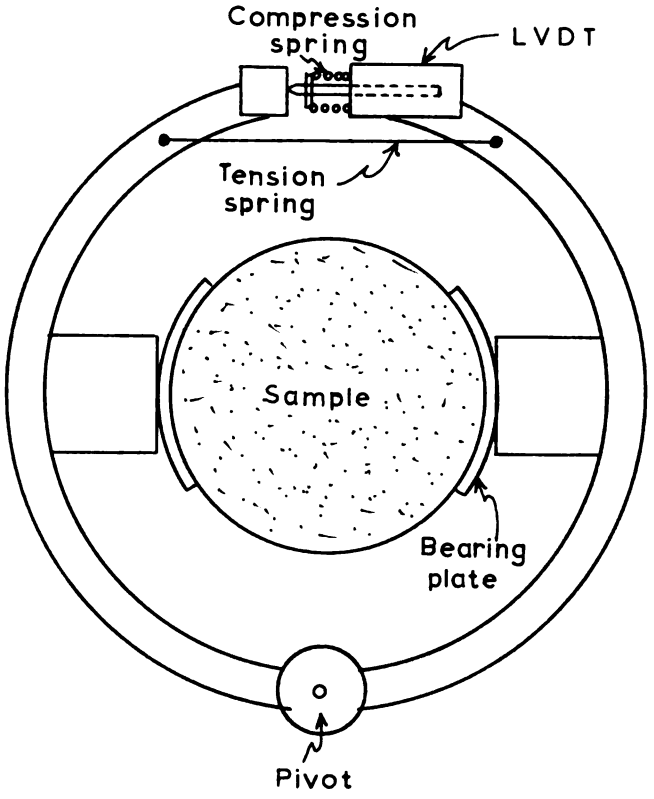

Fig. 4.-- Diagram of radial strain measuring device

The electronic devices used to measure the sample deformations were connected to a Brush, 4-channel, 6KC Carrier Amplifier (Model 13-5443-00) with the output signals being recorded on a Brush Light Beam Oscillograph (Model 16-2308-00).

The temperature inside the soil sample was measured with an iron-constantan thermocouple and recorded on a Varian Graphic Recorder (Model G-14).

The pulsating pressure for the triaxial cell pressure and axial load was supplied by two pulsating pressure cells as shown schematically in Figure 3. Each of these consisted of a piston and cylinder which were linked mechanically with a rotating cam. The pivot point of the mechanical linkage could be shifted to provide different pulse magnitudes. The cams for both cells were connected to a common drive axle by means of electric, magnetic clutches. This enabled the relative phase of the two pulses to be varied. Either one could be disengaged if only one of the loads were to be pulsed. The common drive axle was driven by a ½ H.P., D.C. motor with a variable frequency control. The loading system described produced a sinusoidal cyclic stress with a usable cyclic frequency range from approximately 2 to 30 cps; however, due to the dynamics of the system, the best results could be obtained at approximately 10 cps.

The theoretical natural frequency of the soil sample and its loading system was estimated and found to be much

higher than the frequencies to be used. This was also confirmed from the force-displacement-frequency relationships observed during the testing program. For a given soil sample and a given pulsating axial force amplitude, the resulting axial strain amplitude of the sample was independent of the pulse frequency for the frequency range of 2-30 cps used in these tests. This is what would be expected if the imposed forcing function has a frequency much lower than the natural frequency of the system.

Since air-dry sand was used in the tests, the sample volume change was determined from the amount of air entering or leaving the sample. This was accomplished by means of a device described by Bishop and Henkel (10) with which the air pressure is maintained at atmospheric so that the compressibility of the air need not be considered. This device did not permit measuring the volume change occuring during a given cycle of loading, but it did give the average volume change of the sample over a given period of time. The sample volume changes could also be calculated from the measured lateral and axial sample deformations. This not only provided a check on the measured volume change, but provided a means to determine the volume change occuring during a given cycle if this were desired.

2.2 Soil

Air-dry Ottawa sand was used in the majority of the tests because of its widespread availability. It had a gradation as shown by curve A in Figure 5. Three different initial relative densities were used in the testing program which are called loose, medium, and dense sand in subsequent discussions.

The loose sand was at the maximum void ratio which could be consistantly obtained, and the dense sand was formed by compacting the sand with a rod and tapping the sample mold. This resulted in the minimum void ratio attainable for the material. The specimens considered as loose had a range of void ratios from 0.599 to 0.620 with the average being 0.607, those of medium relative density had a void ratio range of 0.560 to 0.575 with the average being 0.567, and those considered as dense had a void ratio range of 0.521 to 0.540 with the average being 0.533.

The maximum and minimum void ratios which could be obtained by placing this material in a rigid metal container were 0.700 and 0.520. Using these values for e_{max} and e_{min}, and defining relative density as $100(e_{max}-e)/(e_{max}-e_{min})$, the relative densities for the average void ratios given above become 52%, 74%, and 93% for the loose, medium, and dense specimens respectively.

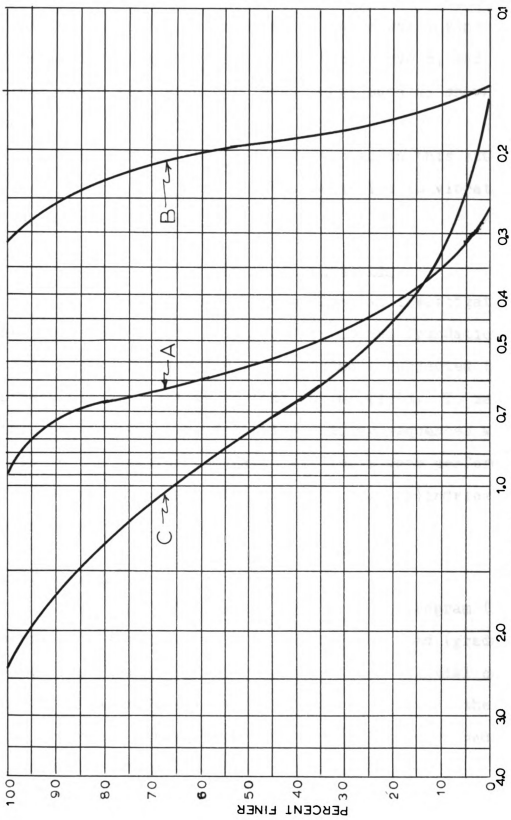

Fig. 5.-- Grain size distribution curves

Later in the testing sequence, two other sands were used for various reasons. One of these was a fine Ottawa sand with a gradation shown by curve B, and the other was a well graded, clean, brown sand as shown by curve C in Figure 5.

Only cohesionless soils were used in this study since this type of soil is more sensitive to vibratory loading than cohesive soils.

2.3 Testing Procedures

If the results of the experimental investigation are to be applied to a dynamically loaded foundation, it is necessary to have the soil specimens subjected to a stress history similar to that in the field. To meet this requirement, the following loading sequences were used in the testing program. All tests were performed on 1.4" diameter by approximately 2.8" high cylindrical specimens.

Test series A

In the primary phase of the testing program (test series A), specimens of air-dried Ottawa sand (gradation A) were first loaded hydrostatically in the triaxial cell to the desired confining pressure, σ_c. Throughout the testing program a confining pressure of 20 psi was used. This is shown as stage I of the loading in Figure 6.

After application of the hydrostatic pressure, the axial stress on the specimen was increased until the desired static principal stress ratio, $R_s=(\sigma_1/\sigma_3)_s = (\sigma_s/\sigma_c)$,

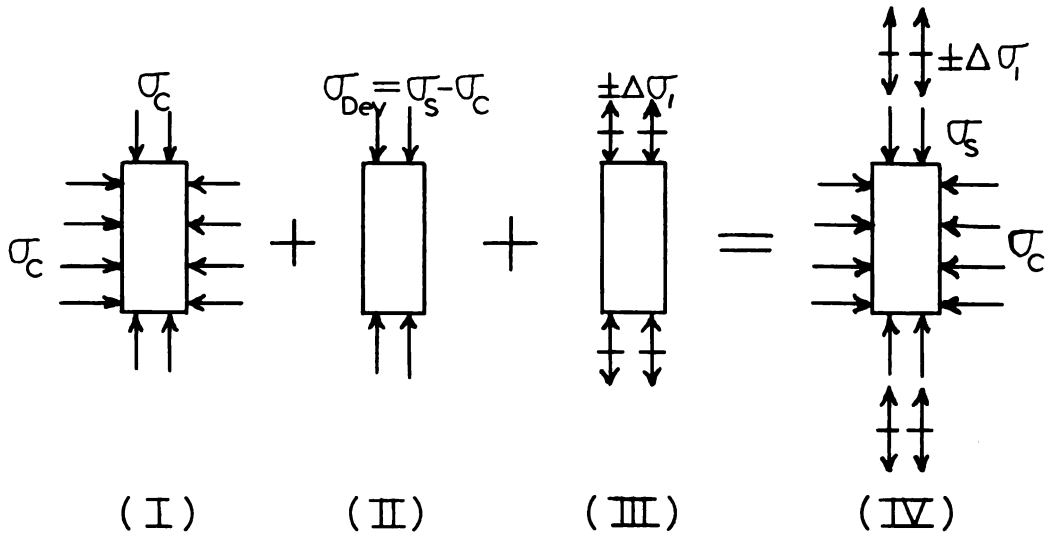

Fig. 6.--Loading sequence

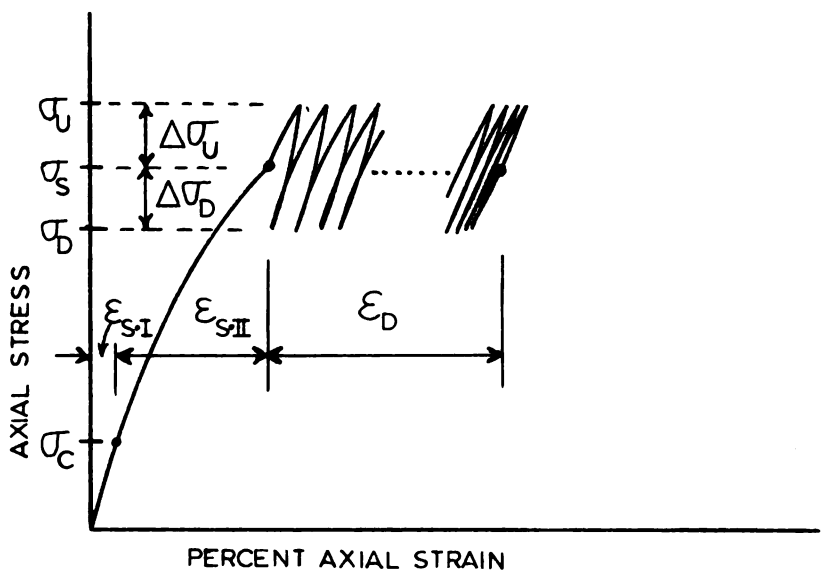

Fig. 7.--Stress-strain curve for loading squence

was attained as shown in Figure 6 as stage II. The specimen was allowed to remain in this condition until there was no appreciable increase of deformation with time.

In the third stage, a cyclic stress was superimposed upon the existing static stress state. For the first phase of the experimental investigation, a cyclic axial stress, $\pm\Delta\sigma_1$, was superimposed on the existing static stress, σ_s. This loading sequence, or stress history, resulted in the combined static and dynamic stress state shown in Figure 6 as stage IV.

Figure 7 shows the axial stress-strain curve for this type of loading condition. During the first stage of loading, the application of the confining pressure, σ_c, caused an axial strain, $\epsilon_{s\cdot I}$. The application of the deviator stress, giving a total axial stress, σ_s, caused an additional static axial strain, $\epsilon_{s\cdot II}$. The superposition of the cyclic axial stress, $\pm\Delta\sigma_1$, (shown in Figure 7 as $+\Delta\sigma_U$ and $-\Delta\sigma_D$ as a more general notation) gave a resulting axial strain of ϵ_D.

Although the axial strains as well as the lateral and volumetric strains were measured for all stages of loading, the strain from the cyclic dynamic loading, ϵ_D, was of primary concern in this investigation.

A third representation of the imposed stress conditions is shown by the Mohr's circles in Figure 8. During the first stage of loading stress path OA was followed

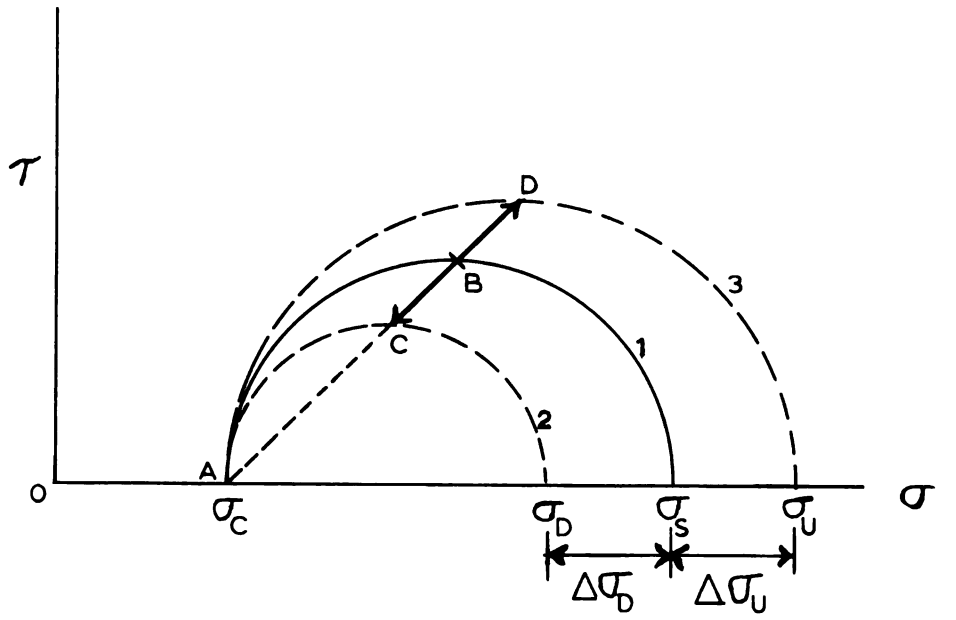

Fig. 8.--Mohr's circles for cyclic axial loading

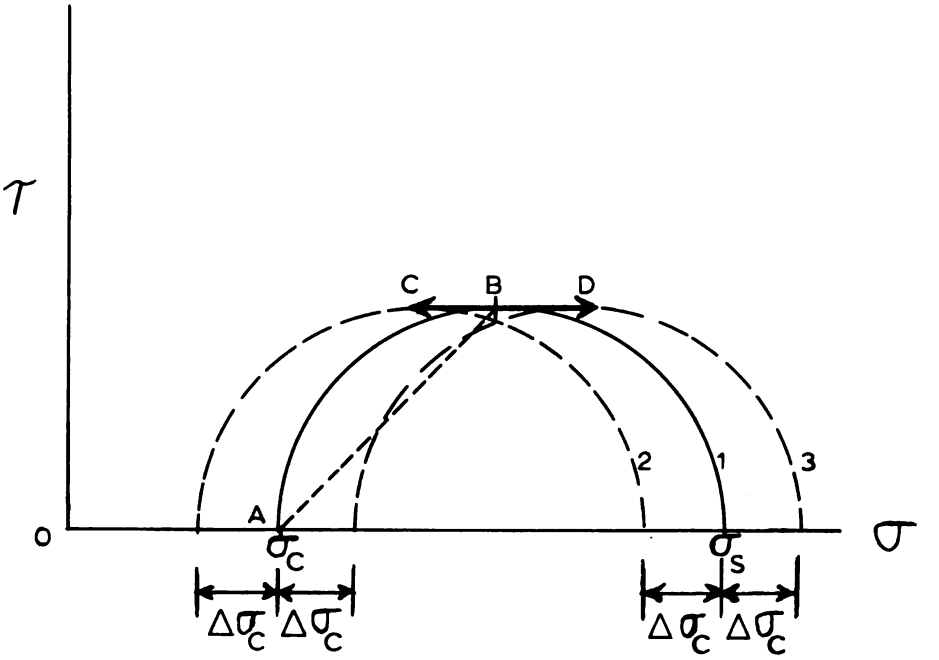

Fig. 9.--Mohr's circles for cyclic cell pressure

until the hydrostatic pressure, σ_c, was reached. During the second stage of static loading, stress path AB was followed until the desired static principal stress ratio, $R_s=\sigma_s/\sigma_c$ was attained. The state of stress on the specimen at the end of this stage is shown by circle 1. During the cyclic loading, the state of stress in the specimen cycled between circles 2 and 3 as indicated by the cyclic stress path CD. This gave a maximum principal stress ratio of $R_m=\sigma_u/\sigma_c=(\sigma_s+\Delta\sigma_u)/\sigma_c$ and a minimum principal stress ratio of $R_n=\sigma_b/\sigma_c=(\sigma_s-\Delta\sigma_b)/\sigma_c$.

Test series B

A variation in the stress history was introduced to examine the effects of stress path on the dynamic strain response. In this series of tests, (series B), stages I and II remained the same as in series A, but stage III was changed. This is indicated by the Mohr's circles in Figure 9. The application of the hydrostatic stress (stage I) is shown by OA and the stress path for stage II is given by AB as before. The cyclic stress was then superimposed by pulsing the cell pressure by an amount $\pm\Delta\sigma_c$. This is indicated by the cyclic stress path CD in Figure 9. The stress state in the sample at the end of the static loading is given by circle 1. Circles 2 and 3 indicate the application of the cyclic stress. This gave a maximum principal stress ratio, $R_m=\frac{\sigma_s-\Delta\sigma_c}{\sigma_c-\Delta\sigma_c}$ and a minimum principal stress ratio, $R_n=(\sigma_s+\Delta\sigma_c)/(\sigma_c+\Delta\sigma_c)$.

Test series C

A second variation in stress history was used to further explore the stress-deformation response. In these tests (series C), stages I and II of the loading sequence remained the same; however, during stage III, the cyclic axial stress was not symmetrical with respect to the static axial stress, σ_s. That is, $\Delta\sigma_U$ and $\Delta\sigma_D$ (as shown in Figure 7) were not equal as they were in series A. These tests indicated the relative importance of $\Delta\sigma_U$ and $\Delta\sigma_D$ and their combined effect upon the dynamic strain, ϵ_D.

Test series D

In test series D, the effects of a static prestress were investigated. This involved altering Stage II of the loading sequence. After the application of the hydrostatic stress (stage I), the deviator stress equal to the total axial prestress of σ_P was applied (Figure 10). After the specimen had reached equilibrium under this static stress condition, the axial stress was reduced to σ_s. Stage III was then initiated. A symmetrical cyclic axial stress was applied as in series A. Most of the tests in this series were performed with the prestress, σ_P, being equal to the maximum stress, σ_U, of stage III. An additional test was performed in this series with σ_P being greater than σ_U.

The conduct of these tests deviated from that of previous tests in one additional manner. After 10,000

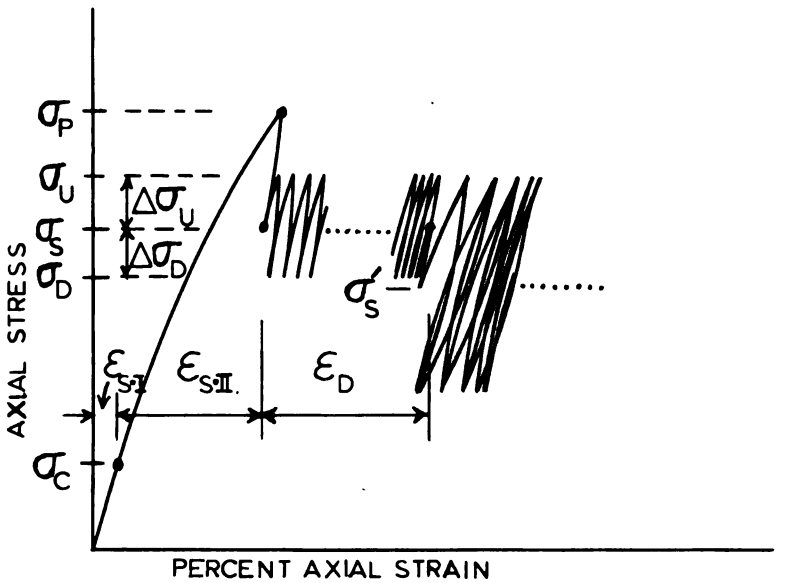

Fig. 10.--Stress-strain curve for prestress loading sequence

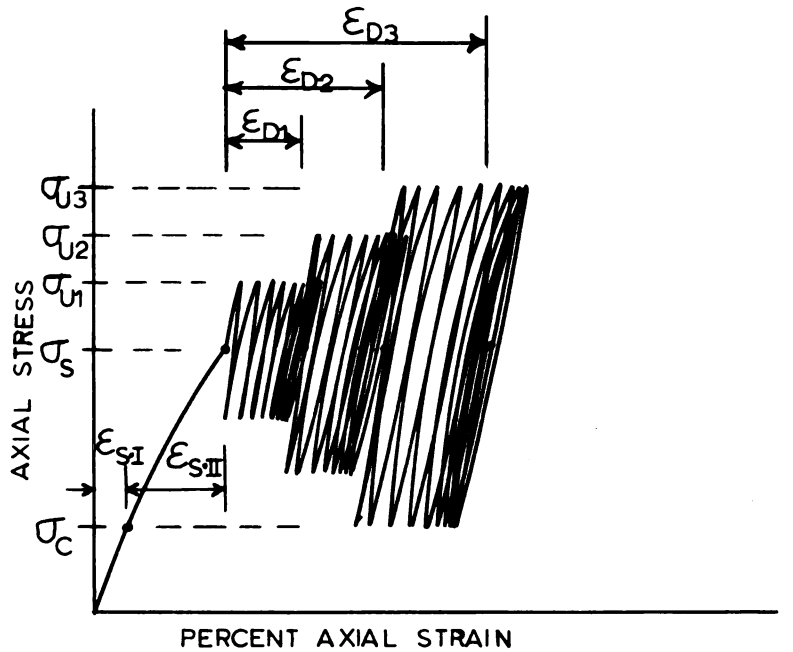

Fig. 11.-- Stress-strain curve for cumulative loading sequence

stress cycles, the static axial stress was again reduced to σ_s' , and a larger cyclic stress was applied so that the maximum axial stress, σ_U, remained the same. This stress change was repeated several times. For the last loading of the sequence, the deviator stress was reduced to zero during the unloading part of the stress cycle. The dynamic strain for each loading of the sequence was considered to be the strain for that loading plus the strains from the preceding loadings.

Test series E

During the early part of the testing program, a series of tests was performed in which several loading conditions were applied to the same soil specimen. This was done in order to obtain as much preliminary information as possible from a single specimen so that the characteristic response trends could be determined.

This series of tests used the same loading sequence as test series A. However, after the axial strain under the cyclic stress approached a stationary value (at about 6,000 cycles), the magnitude of the cyclic stress was increased and the resulting axial strain again determined. This process was continued through several stages. The axial strain for a given cyclic stress was considered to be the total axial strain accumulated through all preceding cyclic loadings plus the strain that occurred under the given cyclic stress. This is shown in Figure 11. For the stress σ_{U3}, the strain is ϵ_{D3}.

Test series F

Tests were also performed on sands with gradations shown by curves B and C in Figure 5. These tests were carried out to further explore certain strain characteristics observed in test series A. The loading sequence was the same as the one used in series A.

Cyclic stress frequencies

In the primary phase of the testing program (test series A) and the initial exploratory phase (test series E), tests were conducted using cyclic stress frequencies ranging from 0.1 cps to 25 cps. This was to investigate possible frequency effects on the dynamic strain response. In subsequent test series, frequencies were used that were most compatible with the type of test being conducted. In test series B, a frequency of 6 cps was used, and 10 cps was used in test series C, D, and F.

CHAPTER III

RESULTS OF EXPERIMENTAL INVESTIGATION

3.1 Axial Strain

As previously indicated, the experimental investigation of the dynamic stress-deformation characteristics was primarily based upon test series A and B on air-dried standard Ottawa sand. In these tests, the specimens were first stressed hydrostatically to a cell pressure, σ_c , of 20 psi. A deviatoric stress was then applied to produce the desired static principal stress ratio, $R_s = \sigma_s / \sigma_c$.

After the soil reached equilibrium under this static stress condition, a sinusoidal pulsating stress was applied in two ways. In series A, the cyclic axial stress was symmetrical about the static axial stress. In series B, a cyclic cell pressure was superimposed on the static cell pressure.

The loading and material variables studied during this phase of the investigation were the static principal stress ratio, R_s, the pulsating axial stress amplitude, $\pm\Delta\sigma_1$, the pulsating cell pressure amplitude, $\pm\Delta\sigma_c$, the pulse frequency, f, and the initial void ratio, e_o, of the sand.

All tests were conducted so that the axial, or major principal stress was never less than the lateral, or minor principal stress. This was due to physical restrictions of the loading mechanism.

Typical results

The axial deformations of the soil specimens were measured with a LVDT and recorded on an oscillograph as described previously. This provided a continuous plot of the axial deformation as a function of time or number of stress cycles which resulted from a given stress state. Curves A, B, C, D, and E, in Figure 12 show actual test data obtained in this manner. For convenience, the axial deformation is given as percent axial strain and the number of stress cycles, N, is plotted on a logarithmic scale. These curves show only the accumulated axial strain at the end of each cycle and not the recoverable strain during each individual stress cycle.

These curves indicate that, with increasing time or increasing number of cycles, the soil appeared to stabilize and the axial strain ceased to increase. For this investigation, the strain measured after 10,000 cycles of axial stress was considered as the dynamic strain, ϵ_D, for the given stress state. Several tests carried to 60,000 cycles of stress showed no appreciable increase in axial strain beyond 10,000 cycles.

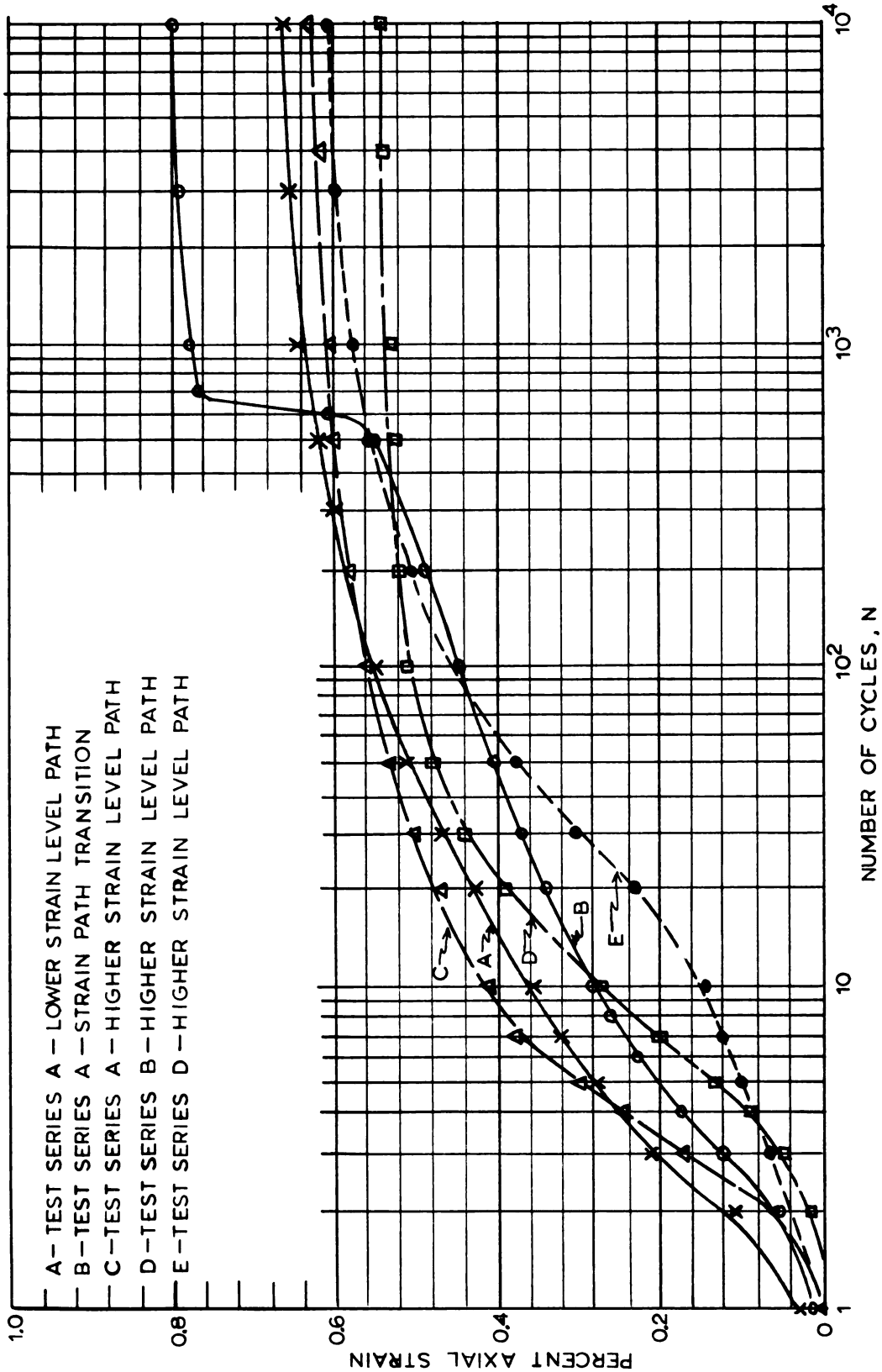

Fig. 12.-- Typical curves of axial strain -vs-number of stress cycles

It was found that the strain for a given stress condition was not unique; furthermore, the dynamic strain occurring for a given material and stress state had two distinct possible magnitudes. This is illustrated by the idealized ϵ-N curves in Figure 13. The two possible strain values are shown in Figure 13 as a lower strain level, ϵ_{DL}, and a higher strain level, ϵ_{DH}. In addition to the two distinct possible dynamic strain levels, there were three possible strain-vs-time curves, or strain paths, which could be followed to reach these strain levels. As shown in Figure 13, the axial strain path could follow ABC which resulted in a lower strain level, ϵ_{DL}; it could also follow ADEF which resulted in a higher strain level, ϵ_{DH}, or it could follow ABEF which started as a lower strain level and at some time made a transition to the higher strain level path.

It was observed during the conduct of the tests that if the axial strain was following the lower strain path, and a transition to the higher level had not taken place by approximately 1,000 stress cycles, a transition would not occur at all. Rather, the strain state would remain stable at the lower level for the remainder of the test. This does not prove, however, that a transition could not occur later if the test had continued.

Further study of the strain-time curves revealed that a definite distinction between the lower and higher

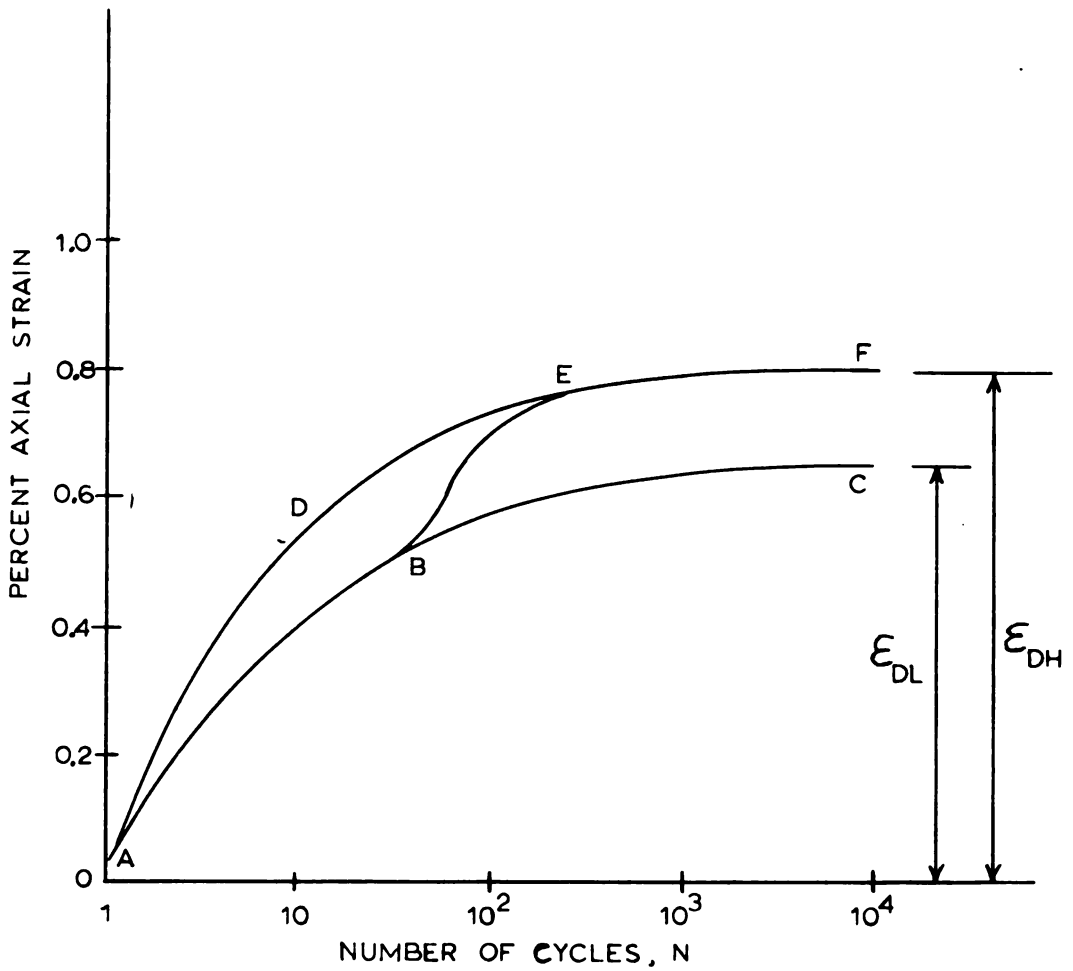

Fig. 13.--Idealized axial strain -vs- number of stress cycles

strain paths could be made by plotting the square of the axial strain-vs-number of cycles. Curves A, B, C, D, and E, in Figure 14 show the typical strain paths from actual data plotted in this manner.

On this type of plot, the lower strain path plotted as a series of three (or occasionally four) straight line segments, as shown by curve A. The higher strain path, on the other hand, plotted as a curve with a continuous change in curvature as shown by curves C and D in Figure 14. Curve B shows a test which had a transition from the lower path at the beginning to the higher path later in the test. The transition phase can easily be seen by the departure from the characteristic straight line plot of the lower strain path when the strain rate increased during the transition to the higher strain path.

This strain-time characteristic made it possible to distinguish whether the dynamic axial strain from a given test was at the high or low strain level without direct comparison with other strain data.

It should be emphasized that although three possible strain paths could be followed in a given test, there were only two possible values for the dynamic strain for that test. This was because both the higher strain path and the path with a transition resulted in the same axial strain. Therefore, these two strain paths may be considered to belong in the same category; the higher strain path represents a transition to the high strain level at the beginning of the test.

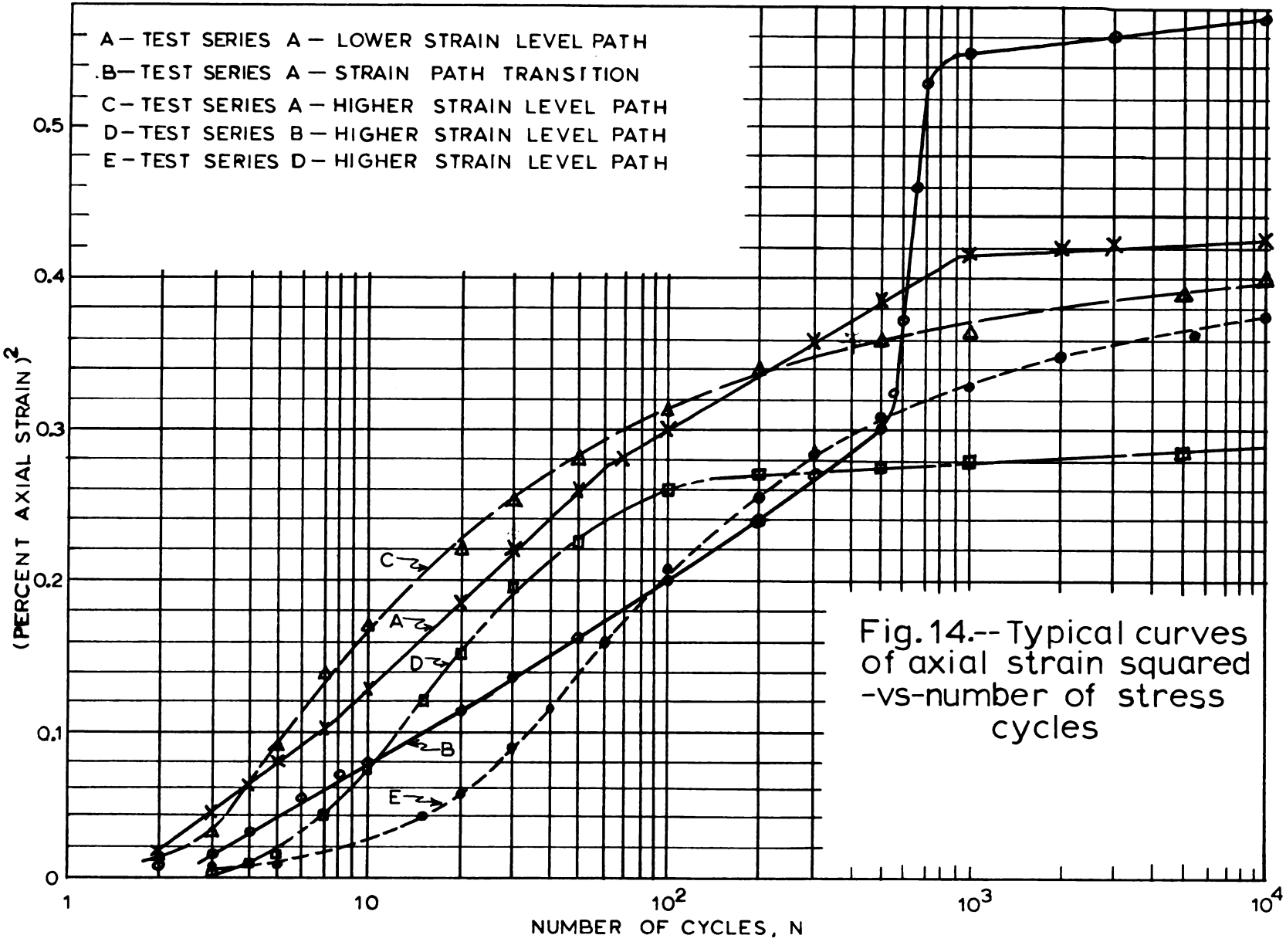

Fig. 14.-- Typical curves of axial strain squared -vs-number of stress cycles

Dynamic-vs-static axial strain

Figures 15, 16, and 17 show a comparison between the static and dynamic axial strains for the loose, medium, and dense sands, respectively. The solid curves in these figures show the static stress-strain relationships.

The results of the dynamic tests are shown by the vertical lines in these figures. The mark near the middle of each line indicates the static principal stress ratio, R_s, of that test. The top and bottom of each line represent the maximum and minimum principal stress ratios, R_m, and R_n, under the cyclic loading. The percent axial strain indicated by each line represents the total axial strain at the end of the test. It is the sum of the strains which occured during the application of the static deviatoric stress and the cyclic stress. The dynamic axial strain, ϵ_D, is the strain difference between the vertical line and the abscissa of a point on the static stress-strain curve at the same value of R_s.

Most of the data show, as would be expected, that the total strain was greater than that which would have been obtained if the principal stress ratio had been increased statically to R_m. There were, however, some exceptions to this. In tests with relatively low R_m values, and particularly in the denser sands, some of

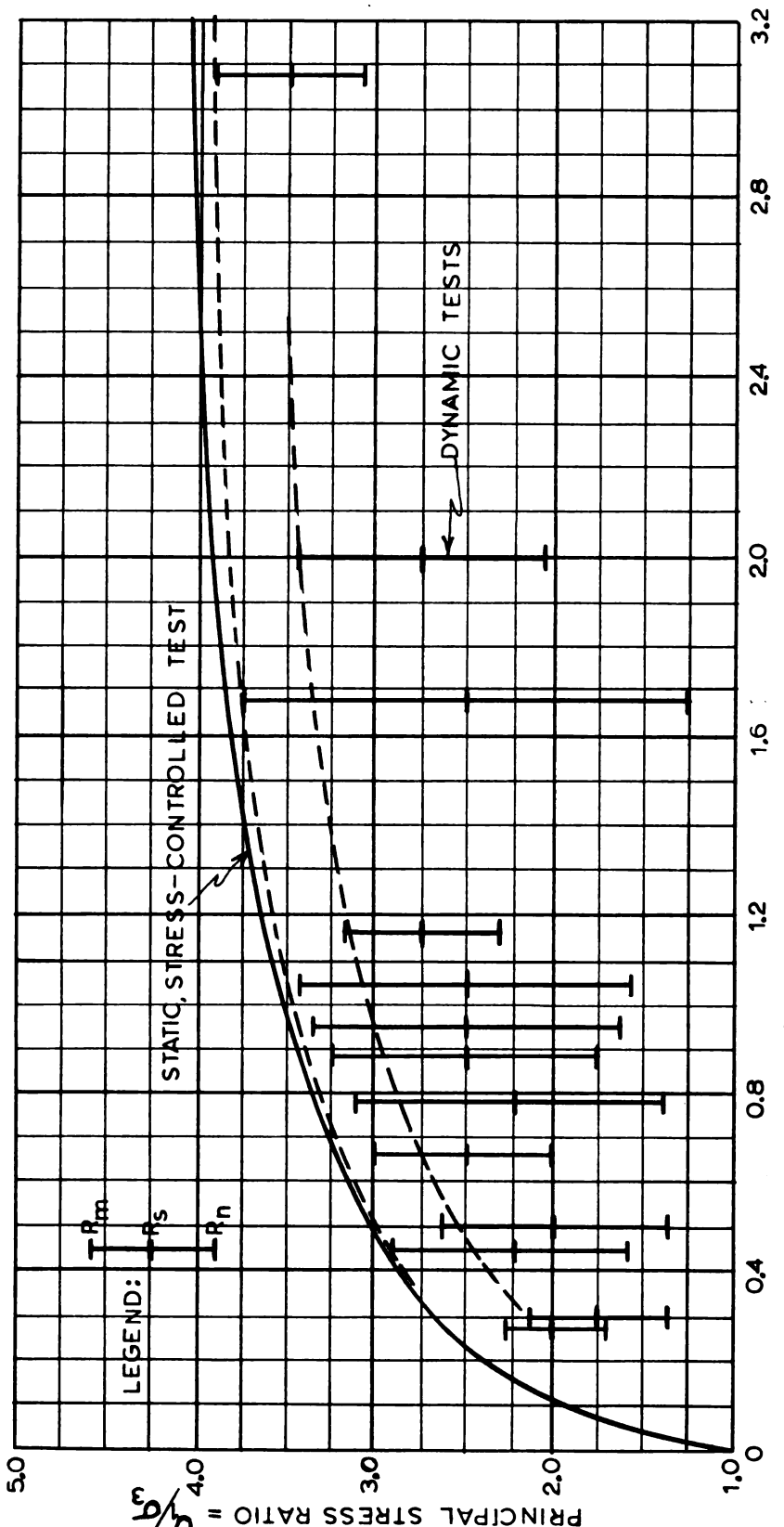

Fig. 15.-- Static-vs-dynamic stress-strain data for loose sand

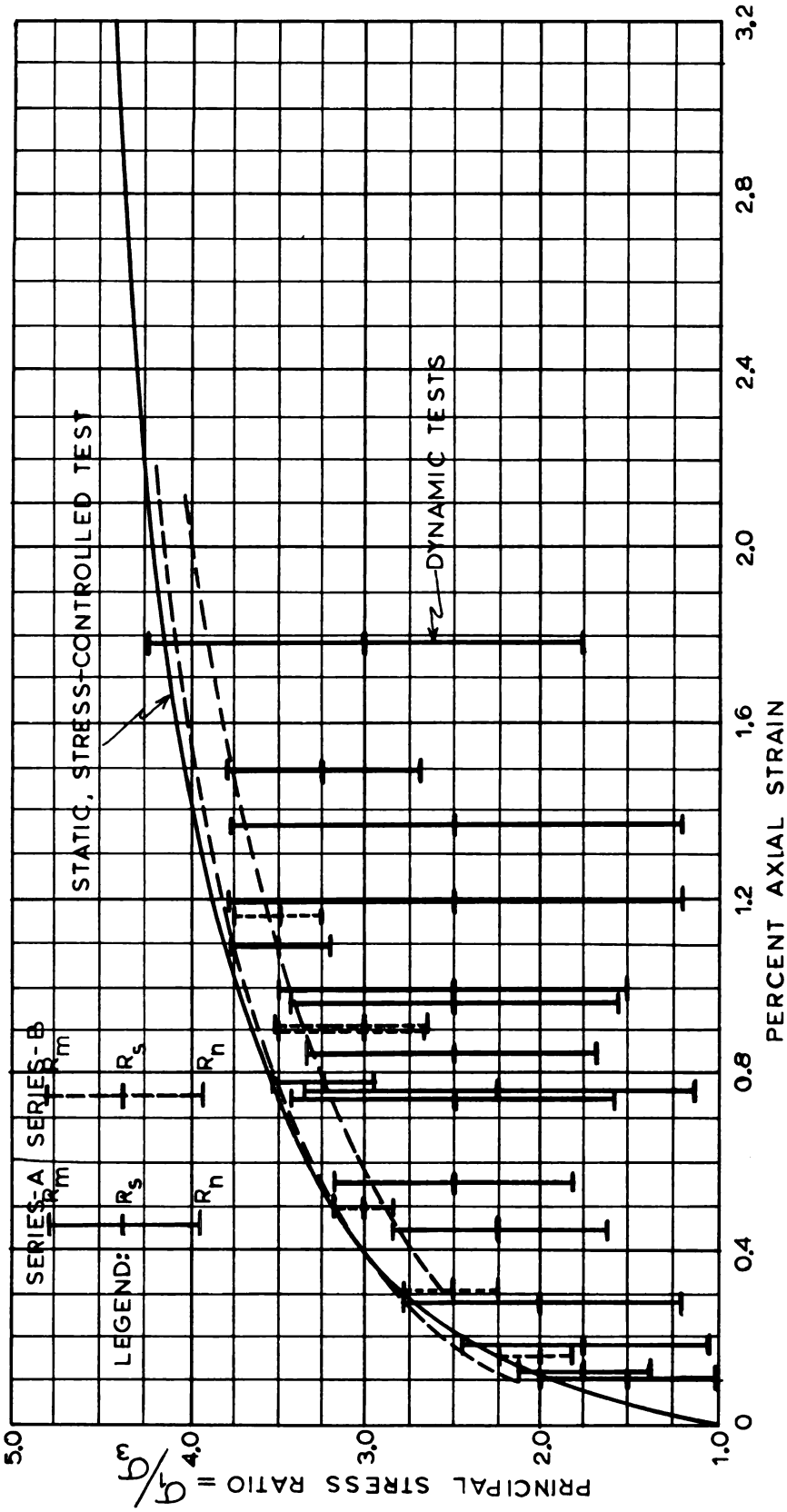

Fig. 16.--Static-vs-dynamic stress-strain data for medium sand

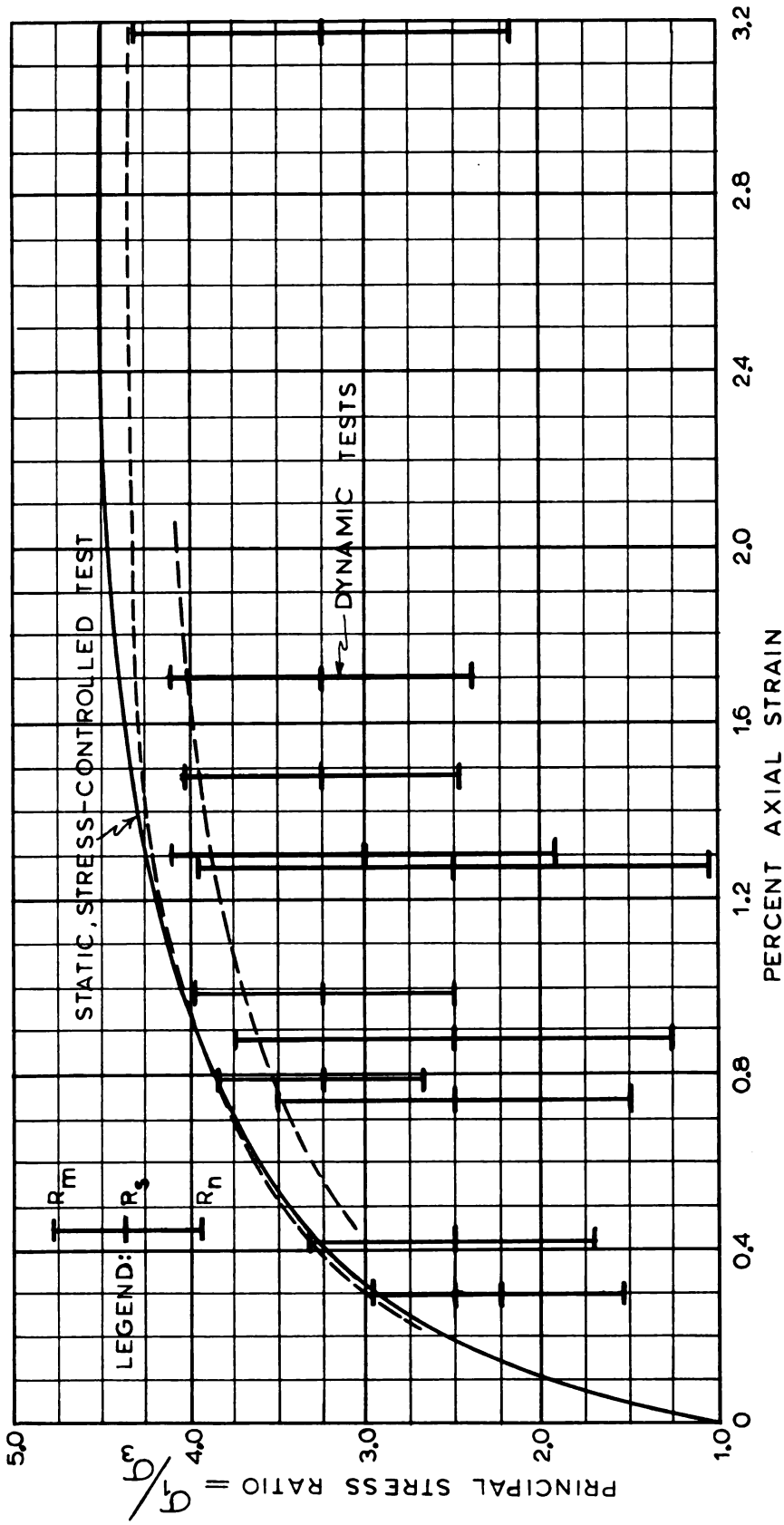

Fig. 17.--Static-vs-dynamic stress-strain data for dense sand

the data show that the strain from a cyclic loading was less than the static strain for the same R_m.

Figures 15, 16, and 17 also indicate that there was not a unique relationship between the maximum dynamic principal stress ratio, R_m, and the resulting dynamic axial strain. Instead, there was a range of possible axial strain values which could result for a given R_m value. This range is shown in Figures 15, 16, and 17 as the zone between the two dashed lines.

It is obvious, therefore, that additional variables must be taken into account if a unique dynamic stress-strain relationship is to be obtained.

Axial strain-vs-stress state

Analysis of the experimental data revealed that for a sand of given initial void ratio, e_o, the dynamic axial strain, ϵ_D, which resulted from the cyclic stress application could be expressed as a function of the imposed stress state. This function involved the maximum principal stress ratio to which the sample was subjected during the cyclic loading, $R_m = \sigma_U/\sigma_C$, and a term $R_D=(R_m-R_s)/R_m$, where $R_s = \sigma_s/\sigma_C$. R_D expressed the ratio of the dynamic stress increase above the static stress to the maximum dynamic stress. A linear relationship was obtained when the axial strain, ϵ_D, was plotted versus the stress factor, F, where $F=R_m{}^3\ R_D{}^{\frac{1}{2}}$.

The plot of the dynamic axial strain-vs-F for the test data is shown in Figure 18. On this plot, two phenomena of particular interest can be observed.

The first phenomenon concerns the two distinct strain levels which have already been discussed. The data shown in Figure 18 clearly indicate that for a given initial void ratio, e_o, and for a given stress factor, F, the dynamic axial strain is one of two distinct values.

The second phenomenon of interest that can be observed in Figure 18 is that for a given initial void ratio, e_o, there is a critical value, F_c, such that below this value, the slope of the F-vs-ϵ_D line is much steeper than the slope above this value. This critical value, F_c, is lower for the higher strain level than for the lower level.

This characteristic is not too surprising in that a similar phenomenon was observed by Barkan (2) with regard to densification of sand. He noted a critical acceleration, below which a given sand at a given void ratio would not densify and above which it would densify to a new void ratio determined by the acceleration to which the sand was subjected.

Okamota, et.al. (29) have reported a similar characteristic for the settlement of a foundation on sand where the entire system was vibrated horizontally

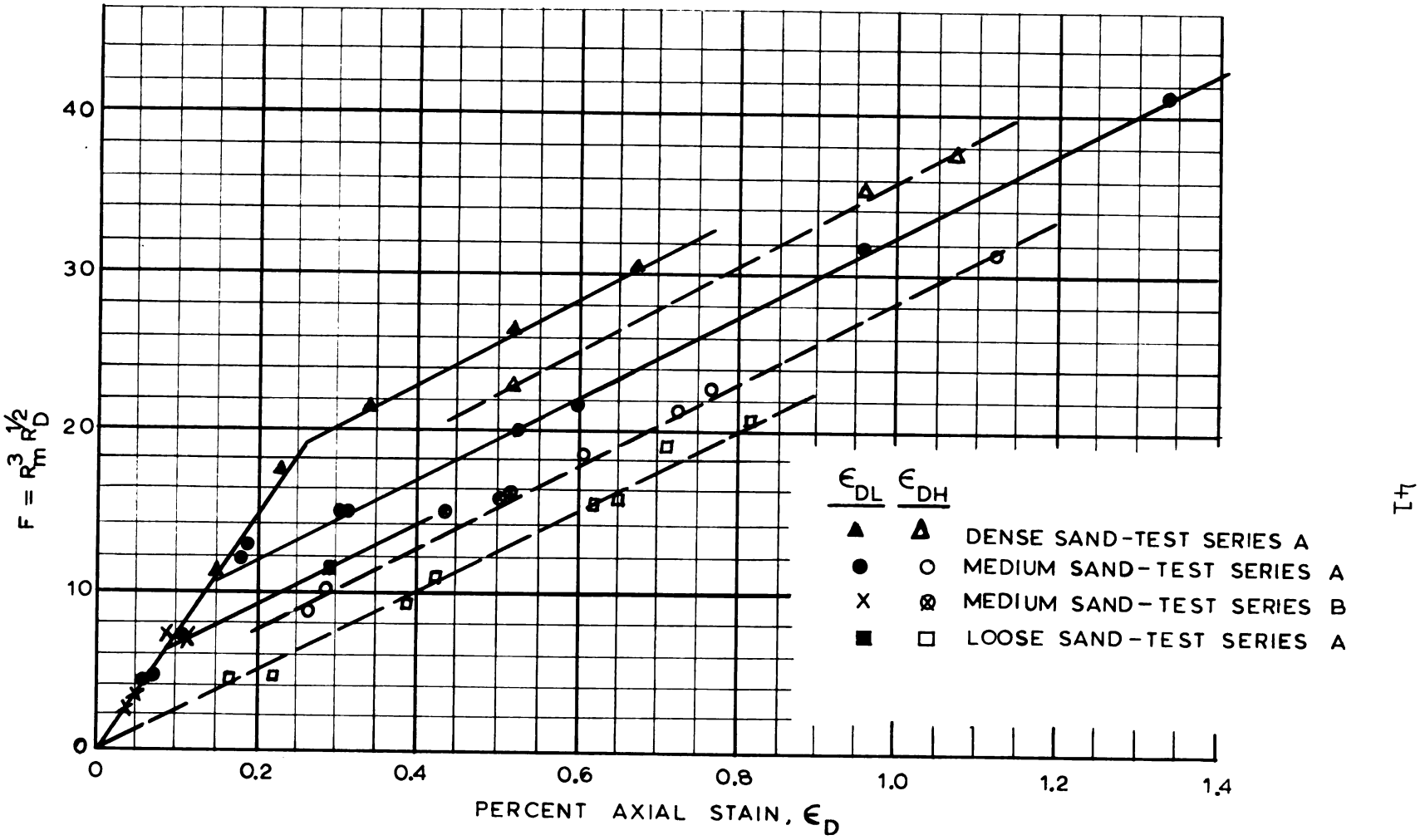

Fig. 18.--Dynamic axial strain-vs-stress state

on a shaking table. They observed only small settlements when the acceleration of the shaking table was below a critical value and large settlements when the acceleration exceeded this value.

In both of these cases, however, the correlation between the "acceleration" imposed upon the system and the actual stresses within the soil mass which caused the deformations were indeterminate. As will be discussed later, the correlation of deformation with acceleration alone is questionable based upon the results of this series of tests. What other investigators have been calling acceleration effects may have been, in reality, stress effects.

The fact remains, however, that for cohesionless soils subjected to cyclic loadings, there apparently exists some type of "threshold" value above which larger soil deformations occur.

Axial strain-vs-void ratio

The effect of e_o on the F-vs-ϵ_D relationship was to shift the curves approximately parallel to each other for values of F greater than F_c. For values of F less than F_c, the dynamic strain was, for all practical purposes, independent of e_o. The value of F_c, however, was dependent upon e_o. It ranged from 0 for the higher strain level of the loose sand to 19.5 for the lower strain level of the dense sand.

Of further interest is the distribution of dynamic strain values between the higher and lower levels for the different initial void ratios. A more complete discussion of this strain level distribution is given in a subsequent section.

Stress path effects

As stated at the beginning of this chapter, this phase of the investigation was conducted by applying the cyclic stress in two different manners. The majority of the tests (series A) were conducted by applying a cyclic axial stress. In test series B, a cyclic cell pressure was used to investigate the effects of the stress path.

Due to physical limitations of the equipment, only a limited number of tests were performed in this manner. However, based on the tests that were performed, there did not appear to be any significant difference between the results of the two types of loading. This fact can be observed in Figure 18 which includes data from both types of loading.

Since these two types of cyclic loading are widely different and most other loading conditions would either be similar to, or would fall somewhere in between these two, it is felt that the dynamic axial strain, ϵ_D can be predicted, for all practical purposes, from the stress factor, F, independent of the stress path, provided there is no prestress.

It is recognized, however, that additional testing must be conducted along this line before a positive conclusion can be reached.

Strain level probabilities

The data from the cyclic loading tests on the standard Ottawa sand were analyzed to determine the frequency of occurrence of high strain levels, ϵ_{DH}. Although insufficient data were available to make a complete statistical study of the results, several definite trends could be noted.

The first characteristic investigated was the probability that either a high level or low level dynamic strain would result from a given stress condition. Figure 19 shows the frequency at which high strain levels, ϵ_{DH}, occurred for a given range of stress factors, F, for each of the three different initial densities. The data include results from test series A, B, and C.

From this figure it can be seen that in general, the frequency of high strain levels increased with increasing F for all sand densities. In addition, these frequencies were dependent on the initial sand density. The loose sand had a high frequency of high strain level occurrences at all stress levels ranging from about 0.75 for F=(0-10) to 1.00 for F=(20-30). The sand of medium density had a much lower frequency of high strain level occurrences ranging from about 0.25 for F=(0-10) to 0.50 for F=(30-40).

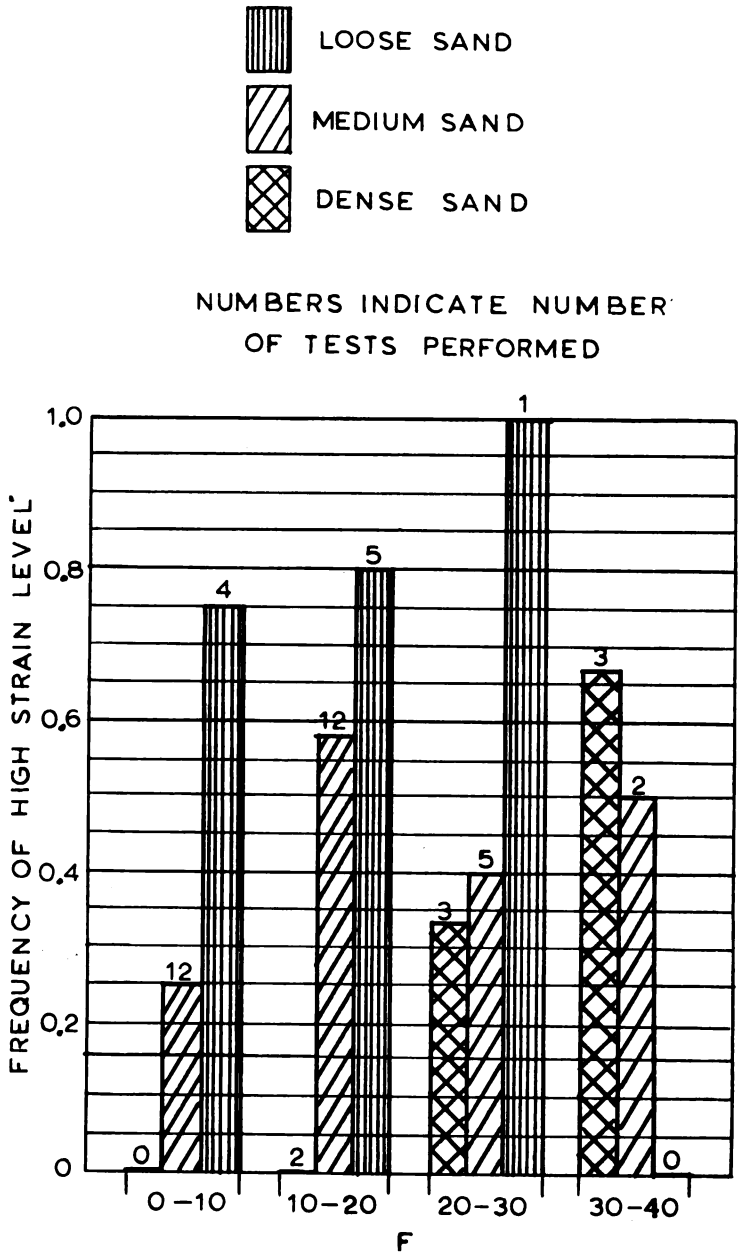

Fig. 19.--Frequency of high strain level-vs- F

For the dense sand, high strain levels were associated with the higher stress factors. There were no high strain level occurrences for F=(10-20), a frequency of about 0.33 for F=(20-30), and 0.67 for F=(30-40).

Since the failure stress factor, F_f, was different for each test and was dependent upon the sand density and the R_D value, the strain level frequencies were also compared on the basis of F' which was the ratio of F to F_f. This is shown in Figure 20. (Failure conditions are discussed in a subsequent section).

Again the frequency of high strain level occurrences increased in general with increasing values of F' as it did for values of F; however, there was one apparent difference. The frequency of occurrence for both the dense and medium sands reached a maximum for F'=(0.50-0.75), and decreased for higher values of F'. Whether this difference reflects actual soil behavior or is simply due to insufficient data is not certain.

The high strain level data shown in Figures 19 and 20 do not distinguish between the two possible strain paths (Figure 13). This characteristic is shown pictorially in Figures 21 and 22.

Figure 21 shows the location of the transition points (in terms of number of cycles of loading) from the low to the high strain path as a function of F. Although most of the high strain levels occurred as a result of a strain path transition, there was no apparent significant

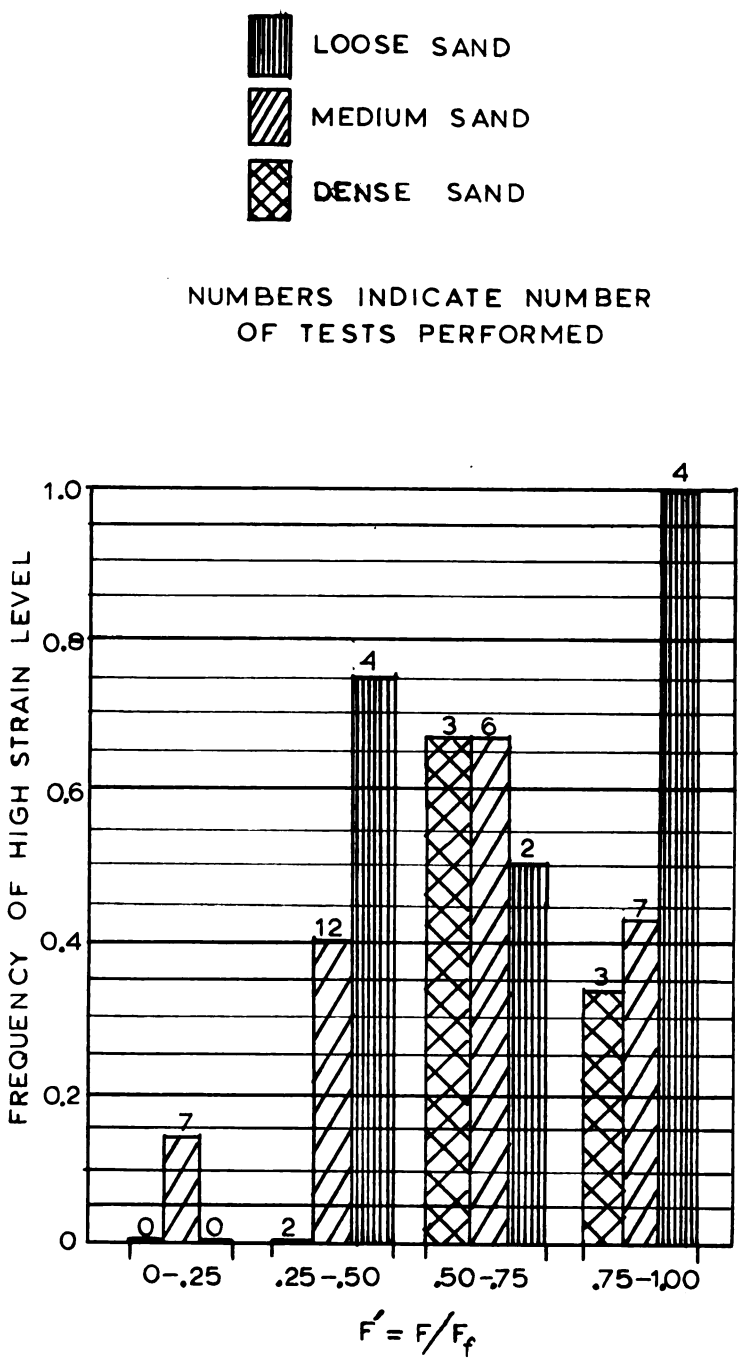

Fig. 20.-- Frequency of high strain level -vs- F'

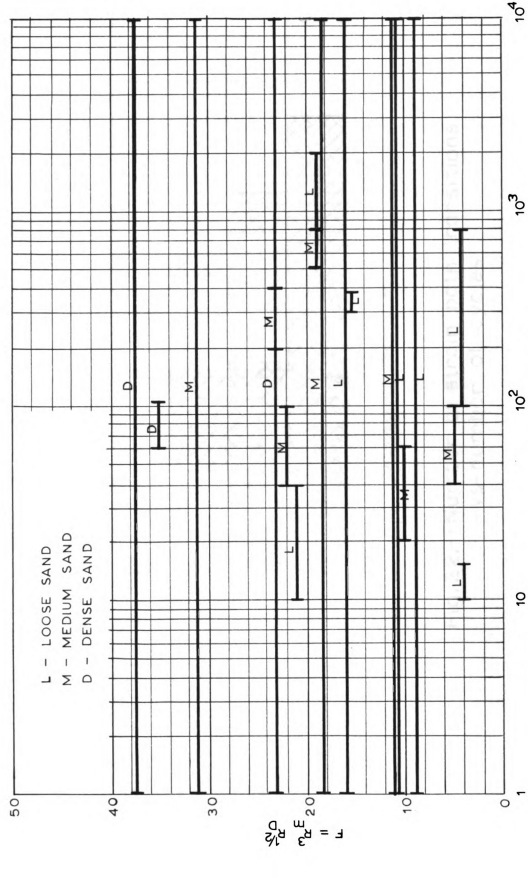

Fig. 21.-- Time of occurrence of strain path transitions

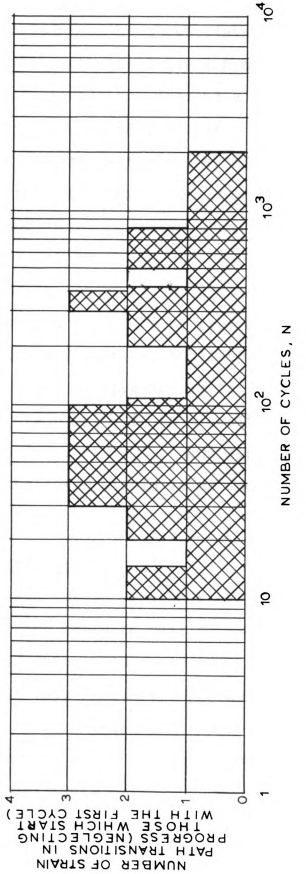

Fig. 22.--Number of strain path transitions -vs-number of cycles

correlation between the stress level and the strain path followed. For both the loose and medium sands, 5 out of 8 high strain levels occurred as a strain path transition, and, for the dense sand 1 out of 3 was a transition.

Figure 22 shows the number of transition points that occurred at various numbers of cycles after the initiation of cyclic loading. As can be seen, there was a slight preference for transitions to occur from about 30 to 100 cycles after the start of the cyclic loading, but the transitions occurred anywhere from approximately 10 to 1000 cycles with about equal probability.

As pointed out previously for tests which followed the lower strain path, if no transitions occurred during the first 1,000 cycles, the sand appeared to remain stable at the lower strain level under continued cyclic loading.

Frequency Effects

A cyclic stress frequency of 10 cps was used for the majority of the tests in this series since the loading system devised for this project operated most satisfactorily at this frequency. However, as mentioned previously, several researchers have attempted to relate soil deformation as a function of the acceleration. In order to investigate this further, other tests were conducted at 2.5, 5, and 25 cps.

At all three frequencies the dynamic axial strain

obtained for a given stress factor, F, and a given initial void ration, e_o, was the same as those obtained at 10 cps. The data plotted in Figures 15 through 18 include the data for all four frequencies. Since the characteristics shown in these figures were independent of the frequency, the various frequencies are not identified in these plots.

The maximum input acceleration in a system can be expressed as $A\omega^2$ or $A(2\pi f)^2$, where A is the deformation amplitude of the system, ω is the frequency in radians/time, and f is the frequency in cycles/time. Analysis of the cyclic strain amplitudes of the soil specimens for given cyclic stress amplitudes indicated that the ratios of stress to strain were independent of the frequency through the range of 2.5 to 25 cps. Therefore, the acceleration of the soil particles for a given cyclic stress was directly proportional to the square of the frequency. It is thus obvious that since the axial strain, ϵ_D, was independent of the frequency, it was also independent of the imposed acceleration. Instead, the soil strain was simply a function of the stress state imposed on the soil mass for the stresses and frequencies used in this investigation.

This does not, however, prove that deformation is independent of acceleration for all accelerations. The maximum acceleration in these tests was less than 1/10 the acceleration of gravity, whereas in much of the previous research, the accelerations ranged from

approximately 0.5g to 3.0g.

It should not be concluded that all deformation characteristics were independent of frequency. One characteristic which was definitely frequency dependent was the strain rate, or strain increment per cycle of load. The higher the pulse frequency, the less was the axial strain per cycle. Figure 23 compares the strain rate for a sand of medium initial density tested at five different frequencies. Approximately 48% of the dynamic strain, ϵ_D, was obtained during the first 10 cycles of loading at 25 cps; at 10 cps, 67% was obtained in 10 cycles; at 2.5 cps, 75%; and at 0.1 cps, 82%.

The data for 0.1 cps were obtained from two special tests in which a slow repeated deviator stress was applied manually. These tests were conducted to compare the strain under slow repeated stress with that under a dynamic stress. The axial strains during the cyclic loading for these two tests were 20% and 40% higher than those predicted from the $F-\epsilon_D$ plot for this sand, although the tests were only continued for 200 and 500 cycles respectively.

Another noticeable difference was that under the slow loading the specimens underwent very little volumetric strain while the dynamic tests conducted at the same stress level showed significant densification. (Volumetric strains, in general, are discussed in a subsequent section.) Since the sand densified in the

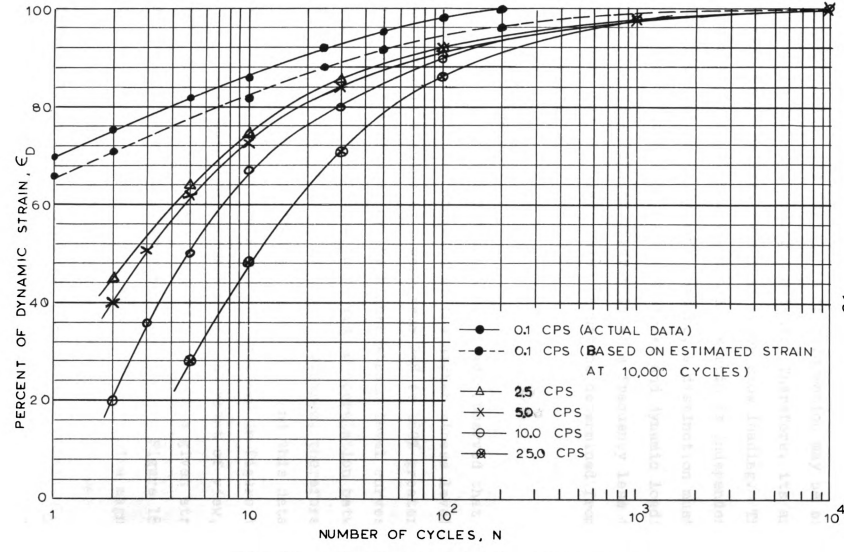

Fig.23.--Dynamic strain rate as function of frequency

dynamic tests, its resistance to deformation may be expected to increase during the test. Therefore, its axial strain would be less than that under slow loading. This indicates that although the axial strain is independent of frequency under dynamic loading, a distinction must be made between slow repeated stress and dynamic loading. This dividing line is apparently at a frequency less than 2.5 cps, but its exact value cannot be determined from the data available.

Failure Conditions

During this investigation, it was observed that for some of the tests conducted at the higher stress levels, the dynamic strains, ϵ_D, were from 25% to 180% greater than those indicated by the higher strain level curves of Figure 18. Furthermore, there was no correlation between F and ϵ_D for this data. It was considered, therefore, that failure had occurred in these tests and this data was considered separately and not included in Figure 18.

It is important, from a practical point of view, to know whether a soil mass when subjected to a given stress state will have a limited strain as shown in Figure 18, or will have a large, finite strain of indefinite magnitude. In this investigation, therefore, failure was defined as having occurred when the dynamic strain, ϵ_D, was greater than that indicated by the appropriate curve in Figure 18.

The plot of axial strain-vs-number of stress cycles for a test in which failure took place looked like the typical curves given previously, except that the dynamic strain was much larger.

Analysis of the failure data indicated that a second critical stress factor, F_f, could be fairly well defined such that for values of F larger than F_f, the correlations of Figure 18 were no longer applicable, i.e., failure would occur. In static triaxial tests, the primary factor controlling failure is the maximum principal stress ratio to which the soil is subjected. For the dynamic loadings, failure also depended upon the value of R_D. This can be seen in Figure 24. This plot shows all the tests in which failure occurred and all the tests in the same range of stress for which failure did not occur.

The stress conditions at which failure occurred appear to be about the same for the dense and medium sand and somewhat lower for the loose sand.

This figure also indicates that the sand could be subjected to higher values of maximum principal stress ratio, R_m, when the value of R_D was also relatively high. The stress ratio at failure could be as high as 4.35, 4.35, and 3.65 for the dense, medium, and loose sands, respectively, if the value of R_D was greater than about 0.3, but the respective values of R_m at failure were 3.80, 3.80, and 3.00 for values of R_D below about 0.125.

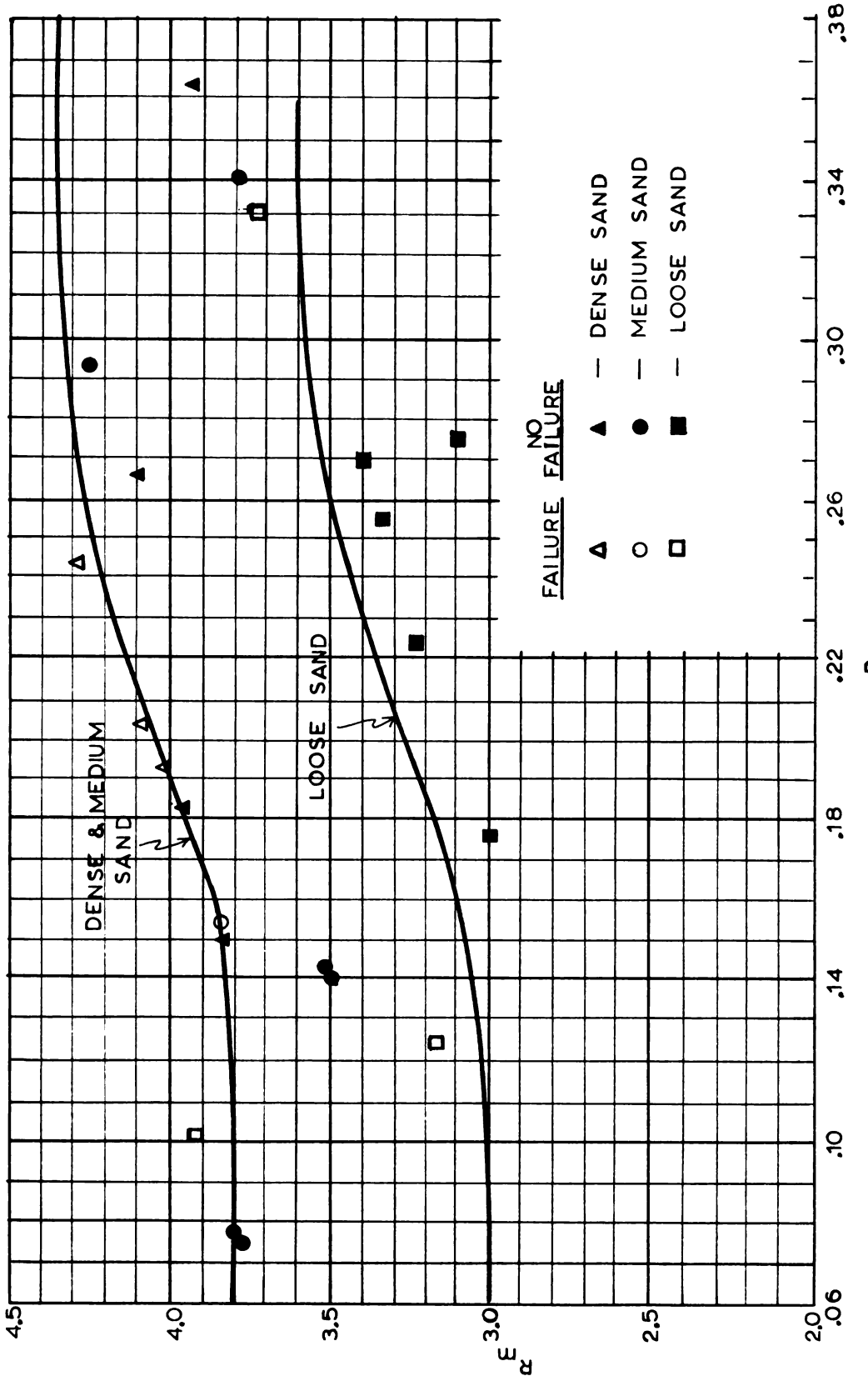

Fig. 24.-- R_m-vs-R_D at failure

These maximum principal stress ratios for the dynamic tests may be compared with the static, stress-strain curves. (Stress-strain curves for static, stress controlled, triaxial tests are shown in Figure 25.) The values of R_m at failure in dynamic tests may be related to the stress ratios in static tests at which plastic deformations become important.

For example, in dynamic tests, the maximum values of R_m were equal to 4.35, 4.35, and 3.60 for dense, medium, and loose sands (Figure 24). It can be noted that the stress ratios corresponding to a tangent modulus of 700 psi in the static tests were 4.35, 4.25, and 3.65 for the dense, medium, and loose sands, respectively.

Also, the stress ratios corresponding to a modulus of 2,500 psi in the static tests were 3.80, 3.70, and 3.00 for the dense, medium, and loose sands, respectively. These values are comparable with the corresponding values of R_m equal to 3.80, 3.80, and 3.00 for dynamic tests (Figure 20, for values of R_D below 0.125).

If yielding of the soil in static tests is considered to be represented by some specified value of the tangent modulus, then the preceding examples would suggest that failure may occur under dynamic loading when R_m exceeds the value necessary to produce yielding.

It should be remembered, however, that the value of R_D has considerable influence on the dynamic failure value

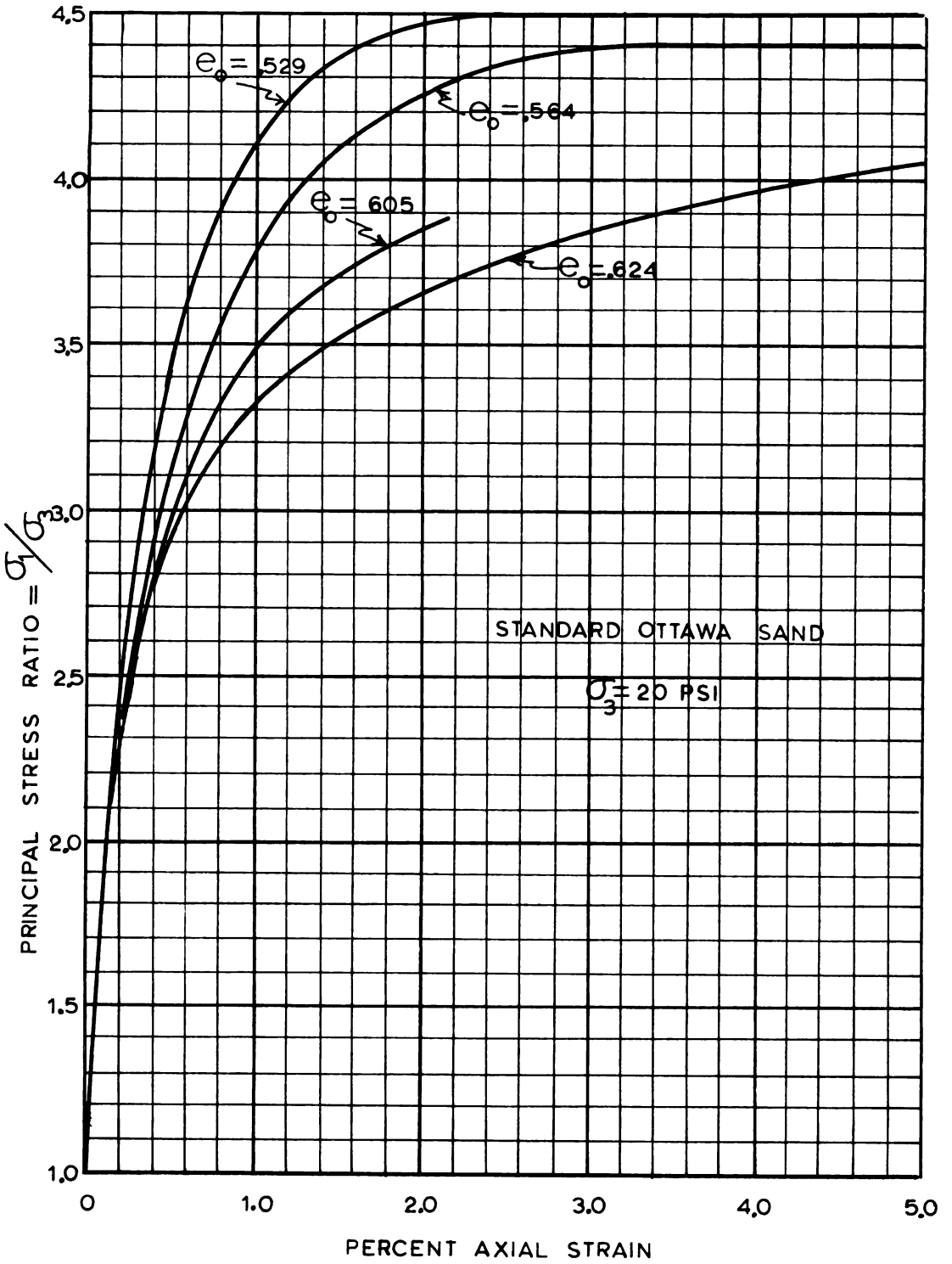

Fig. 25.--Stress-strain curves from static triaxial tests

of R_m. This is further illustrated by Figure 26 which is computed from the data of Figure 24. Figure 26 shows the minimum values of R_D for a given stress factor, F, for which failure does not occur.

For example, when a dense sand was subjected to a combined stress factor, F, of 30.0, if the value of R_D was less than 0.20, failure did occur, and if R_D was greater than 0.20, failure did not occur and the resulting axial strain from the cyclic stress could be predicted from the F-vs- ϵ_D plot of Figure 18.

3.2 Volumetric Strain

Throughout the testing program, in addition to measuring the axial strain of the cylindrical samples, the volumetric strain was also determined. This was accomplished by the two methods described in Chapter II. Further details are discussed in Appendix A. The average volumetric strains from these two methods of determination have been used in the following discussions.

Figures 27, 28, and 29 show the volumetric strain data from the static and dynamic tests for the loose, medium, and dense sands, respectively. The continuous, solid line in each figure shows the percent volumetric strain-vs-principal stress ratio, σ_1 / σ_3, from a static, stress-controlled test. The arrows show the results of the cyclic loading tests. The tail of each arrow gives the value of R_s for that test and the

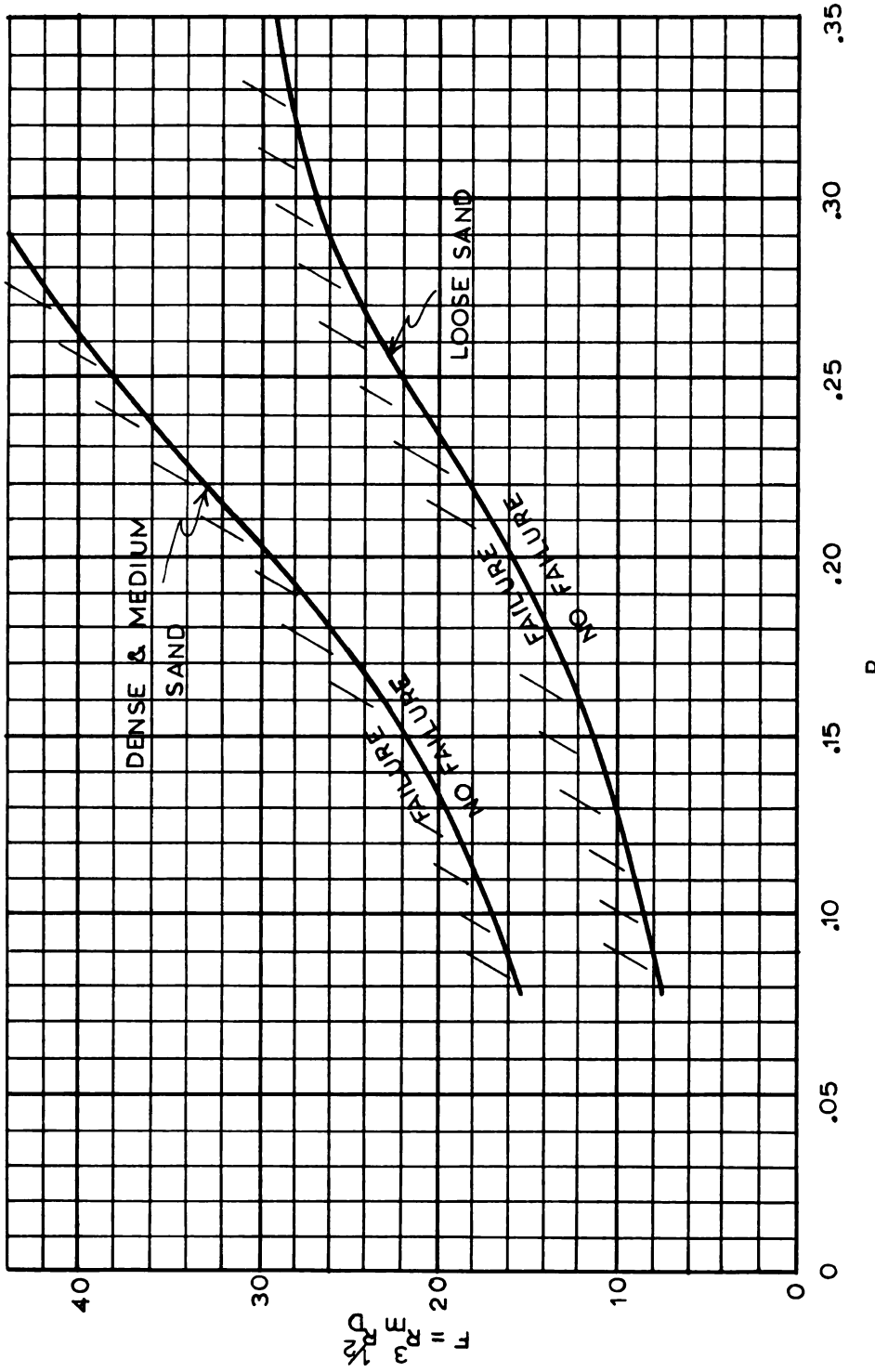

Fig. 26.--Minimum R_D for a given F for which failure does not occur

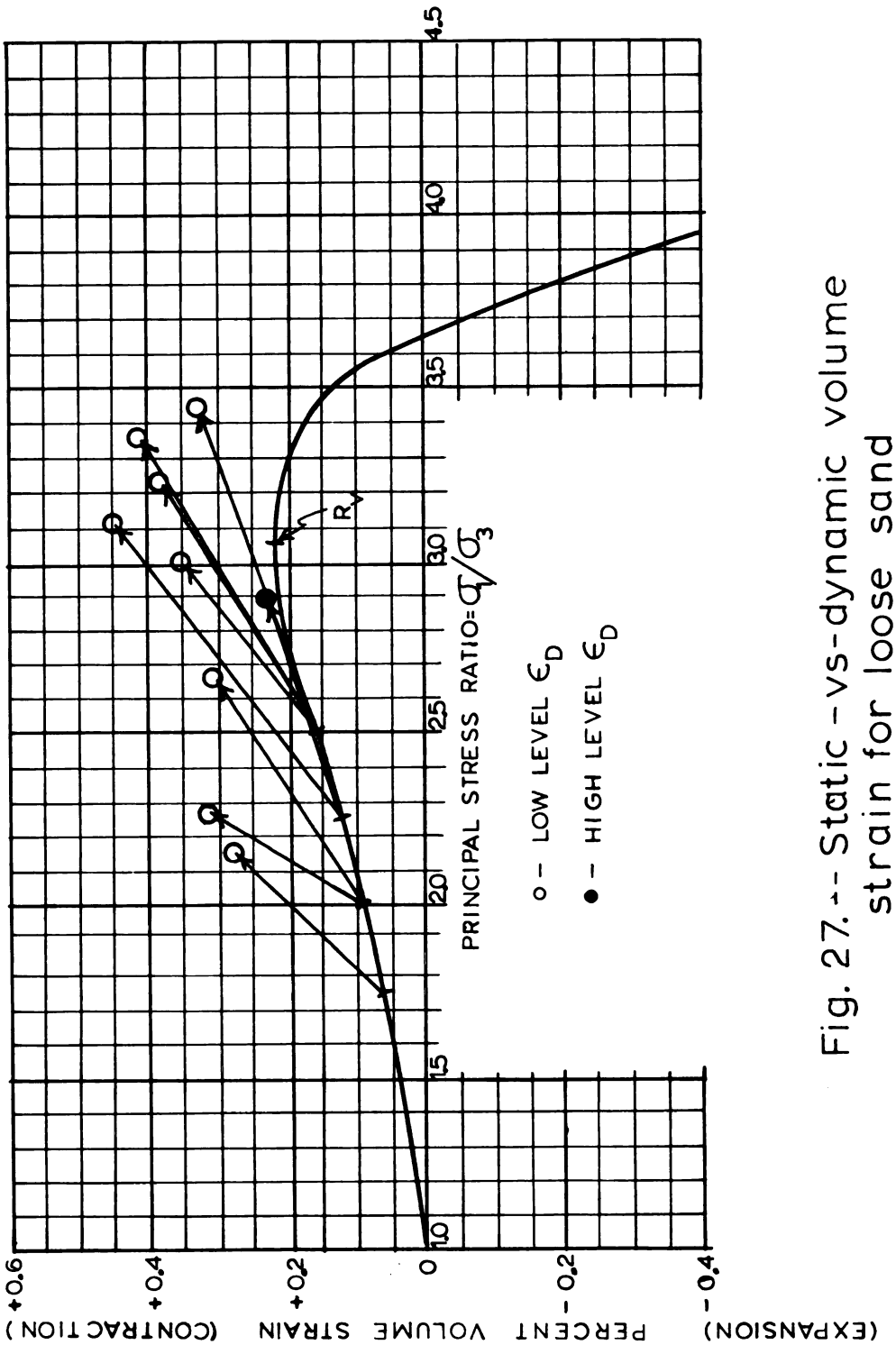

Fig. 27.-- Static-vs-dynamic volume strain for loose sand

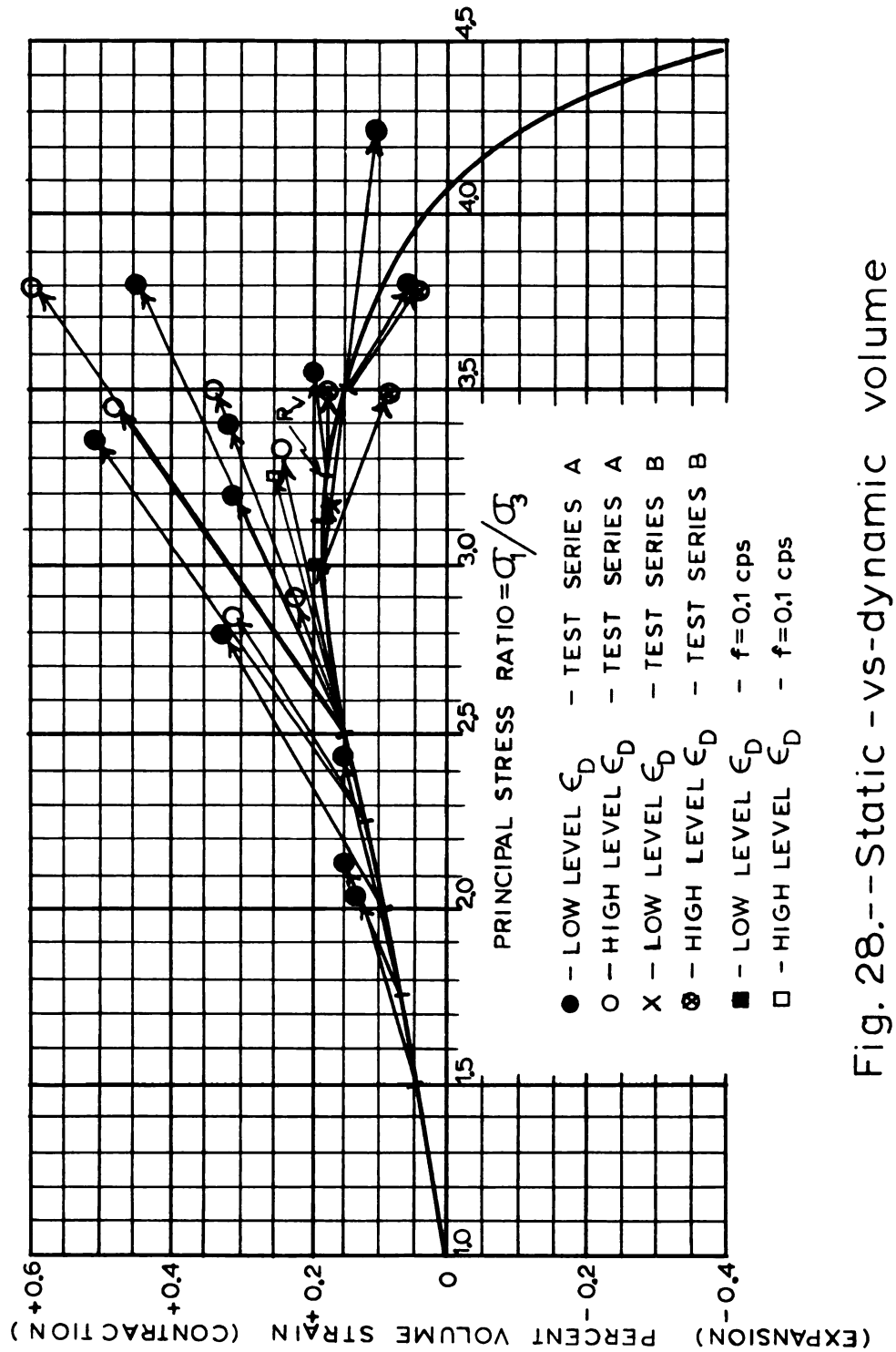

Fig. 28.--Static-vs-dynamic volume strain for medium sand

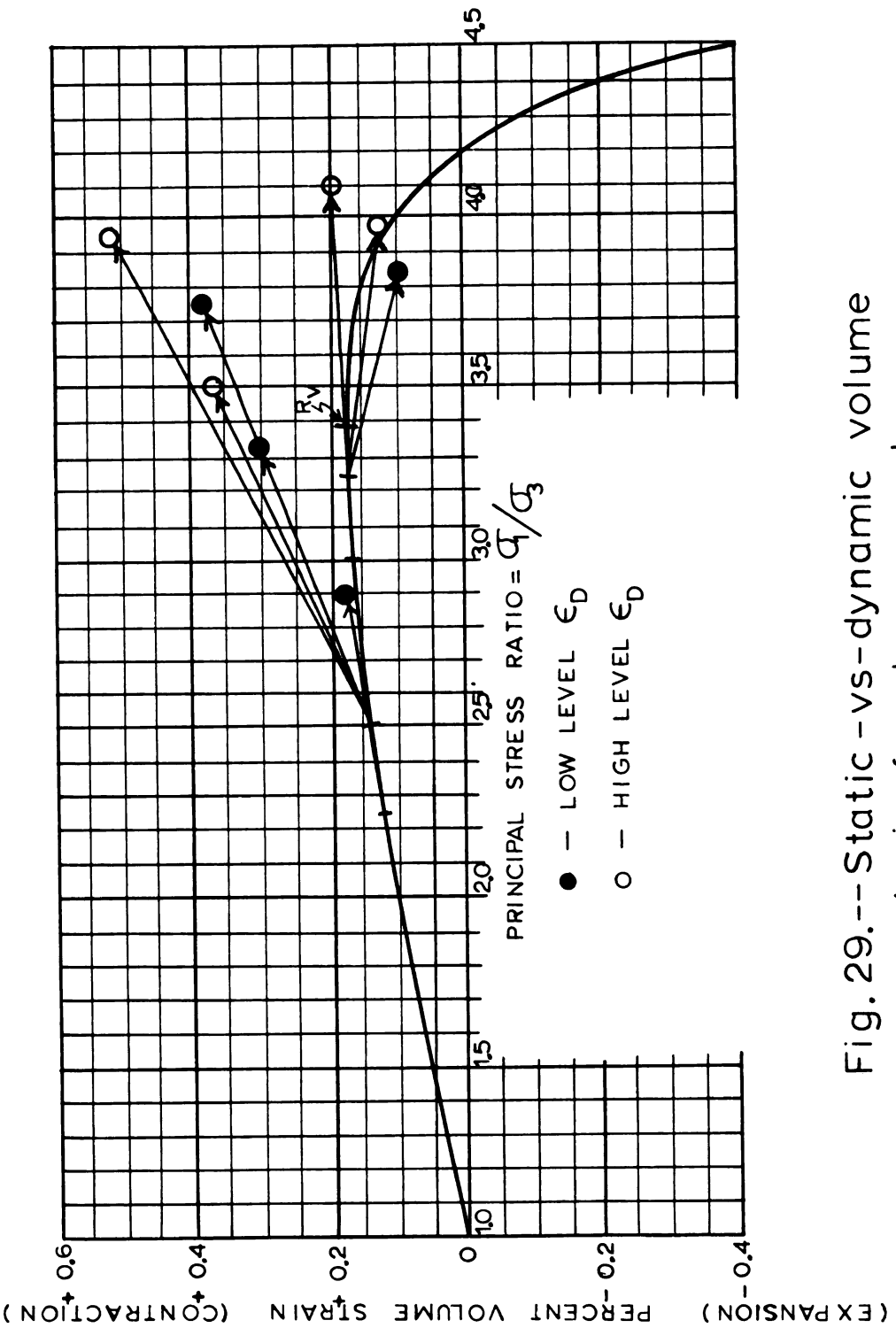

Fig. 29.--Static-vs-dynamic volume strain for dense sand

corresponding volumetric strain attained under that static loading. The tip of each arrow shows the value of R_m for that test and the volumetric strain attained at the completion of 10,000 stress cycles (i.e., the sum of the volumetric strains from the static loading to R_s and the dynamic loading to R_m).

In the static tests on samples at all three sand densities, there was a densification of the sand as the principal stress ratio was increased from 1.0 to a certain value, R_v. As the stress ratio was further increased, the soil began to expand and continued to do so until failure occurred. In the dynamic loading tests, as long as R_s was less than R_v, densification of the sand resulted during the dynamic loading. This was independent of whether R_m was less than or greater than R_v. As can be seen from Figures 27, 28, and 29, the amount of densification was considerably greater than would have occurred if the stress ratio had been increased statically from R_s to R_m. This was true even for the sand which was initially dense.

On the other hand, when R_s was equal to or greater than R_v, the soil expanded during the application of the dynamic loading. All of this expansion, however, occurred during the first 2 to 4 cycles of loading, after which the soil densified slightly for the remainder of the test.

The volumetric strain data is also shown in Figures

30, 31, and 32 where the percent volumetric strain under dynamic loading, ϵ_{vol} , is plotted against R_m. It can be seen that for a given R_s, a curve can be drawn to relate R_m with ϵ_{vol} . For R_s less than R_v, the amount of densification increases with increasing R_m, and for R_s greater than R_v, the amount of expansion increases with increasing R_m.

Although there was considerable scatter in the data, it appeared that tests which had a high level axial strain also exhibited a larger volumetric strain.

There was a significant difference in the amount of densification for the sands at different initial densities. The loose sand showed significant densification at low stresses while the dense sand densified appreciably only at the higher stress levels. This was to be expected. Although there was a distinct difference in the amount of densification between initially loose and dense sand, for a given stress condition the final void ratios obtained for the two densities did not approach each other. For example, the maximum volumetric strain in the tests involving loose sand was approximately 0.4% which corresponds to a change in void ratio of the loose sand from .607 to .601. The same loading condition on a sand of medium density changed its initial void ratio of .567 to a final void ratio of .564.

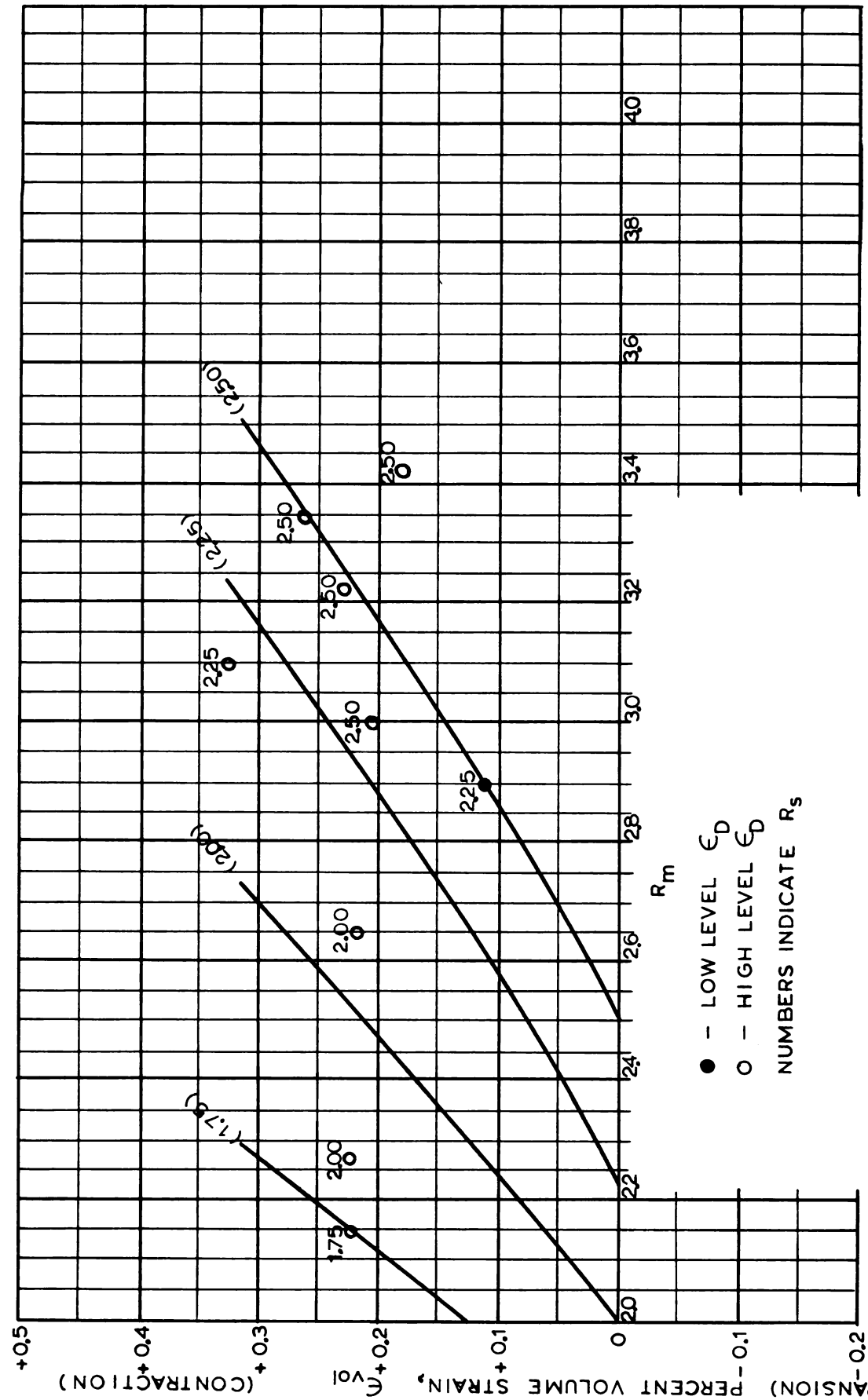

Fig. 30.--Dynamic volume strain for loose sand

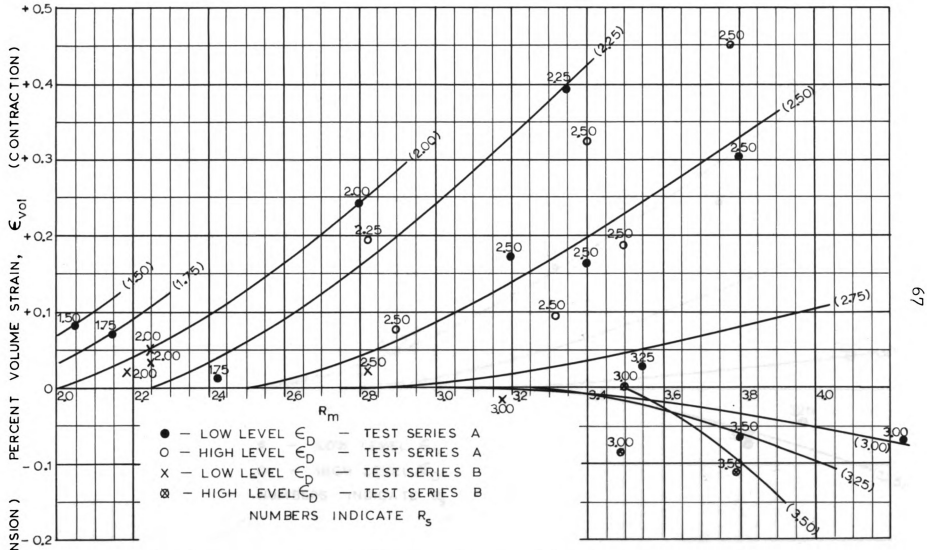

Fig. 31.-- Dynamic volume strain for medium sand

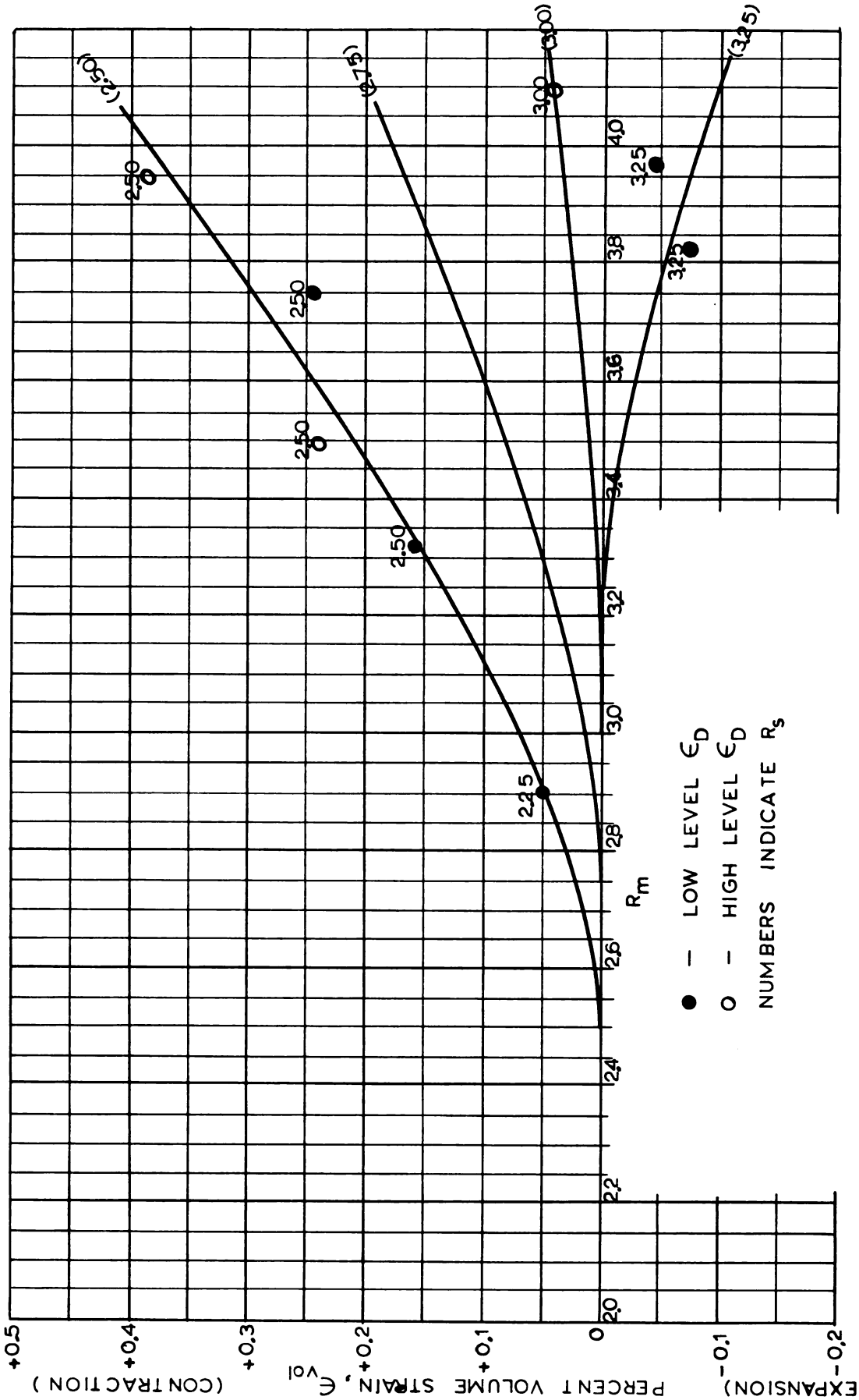

Fig. 32.-- Dynamic volume strain for dense sand

3.3 Contribution of Shearing and Volumetric Deformations to Axial Strain

In order to gain more insight into the stress-strain phenomenon, an attempt was made to separate the axial strain into two components; one due to volumetric deformation and one due to shearing deformation. The volumetric and shear strains of the soil can be written as,

$$\epsilon_{vol} = \epsilon_{DV} + 2\epsilon_{LV} = \Delta V$$

and, $\epsilon_{D\gamma} - \epsilon_{L\gamma} = 2\gamma$

where $\epsilon_{vol} = \Delta V$ =volumetric strain

2γ =shear strain

ϵ_{DV} =axial strain due to ΔV

$\epsilon_{D\gamma}$ =axial strain due to 2γ

ϵ_{LV} =lateral strain due to ΔV

$\epsilon_{L\gamma}$ =lateral strain due to 2γ .

If it is assumed that the volumetric strains are isotropic, i.e., that $\epsilon_{DV} = \epsilon_{LV}$,

then $\epsilon_{vol} = \Delta V = \epsilon_{DV} + 2\epsilon_{LV} = 3\epsilon_{LV}$, or, $\epsilon_{LV} = \epsilon_{DV} = \Delta V/3$.

Also, $\Delta V = \epsilon_D + 2\epsilon_L$,

where ϵ_L =total lateral strain.

Therefore, $\epsilon_{D\gamma} = \epsilon_D - \frac{1}{3}(\epsilon_D + 2\epsilon_L) = \frac{2}{3}(\epsilon_D - \epsilon_L)$

and, $\epsilon_{DV} = \frac{1}{3}(\epsilon_D + 2\epsilon_L)$.

Using the assumption that the average lateral strain of the sand specimen, ϵ_L , was equal to $\frac{1}{2}$ the lateral strain measured at the specimen mid-height (Appendix A), ϵ_D , $\epsilon_{D\gamma}$, and ϵ_{DV} were determined from the data

and plotted against the number of cyclic stress repetitions. Typical plots are shown in Figures 33, 34, and 35.

From these figures, it can be seen that for all densities and strain levels, a high percentage of the total axial strain (75%-95%) was due to shearing deformation.

It can also be seen that in the tests with a transition from the low strain path to the high strain path, the transition is reflected in both $\epsilon_{D\gamma}$ and ϵ_{DV}. Since the volumetric strain is simply $3\epsilon_{DV}$, the transitions would also be noticeable in a plot of ϵ_{vol}-vs-N.

Figure 36 shows the total axial strain-vs-the volumetric strain for the data shown in Figures 33, 34, and 35. The strain path transitions are not reflected in this plot. Hence, the ratio of the volumetric strain to the axial strain appears to be independent of the strain path. This ratio, however, changes with the number of load cycles, with the ratio increasing as the number of cycles increases. It is also dependent on the stress conditions to which the sample was subjected, but appears to be independent of the sand density.

For comparative purposes, data from static loading tests are also shown in Figure 36. As can be seen, the shape of these curves is very different from that of the dynamic tests. Under static stress, as the axial strain increased, there was a tendency of the volumetric strain

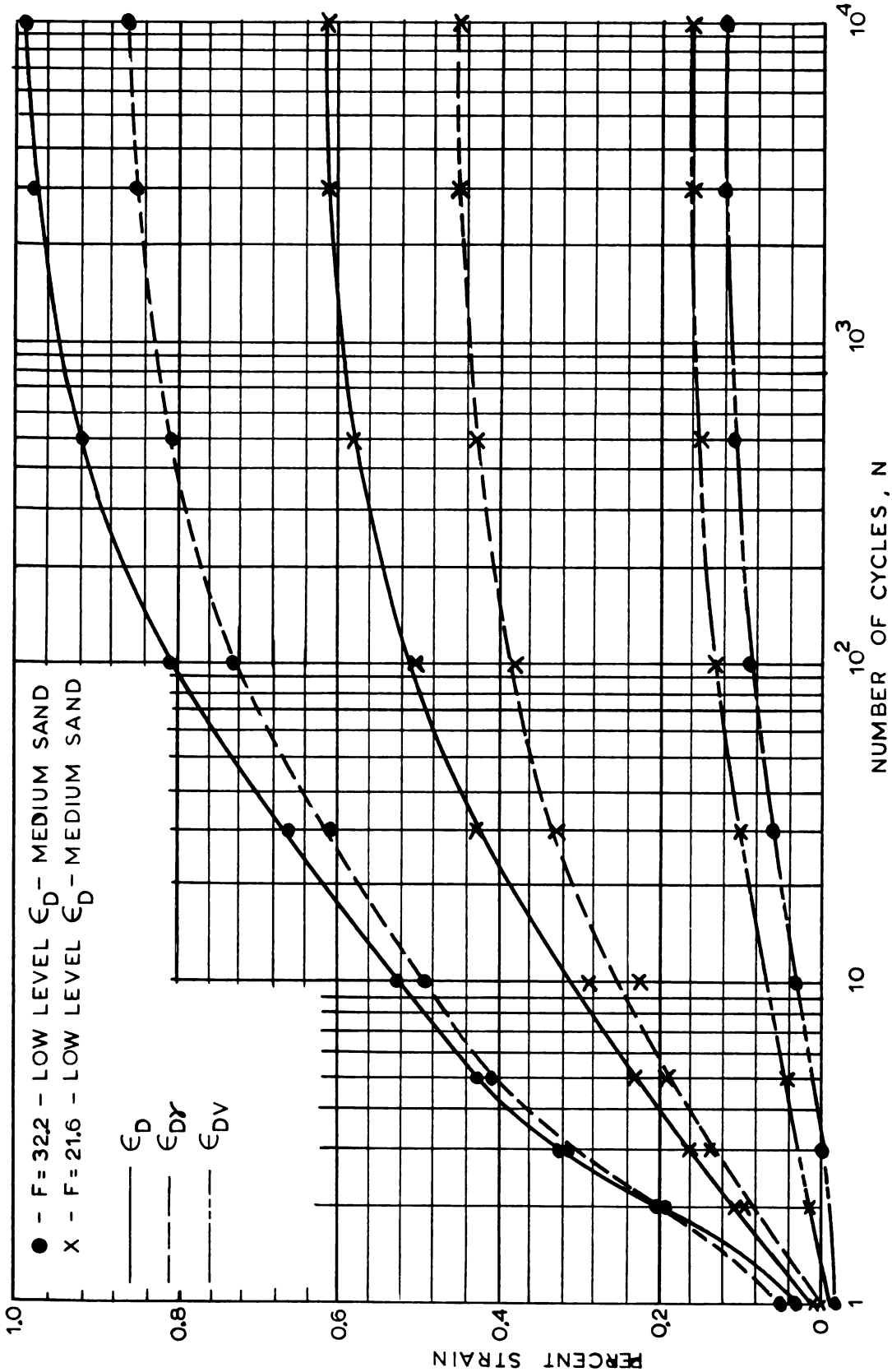

Fig. 33.--Axial strain: shear-vs-volume deformation

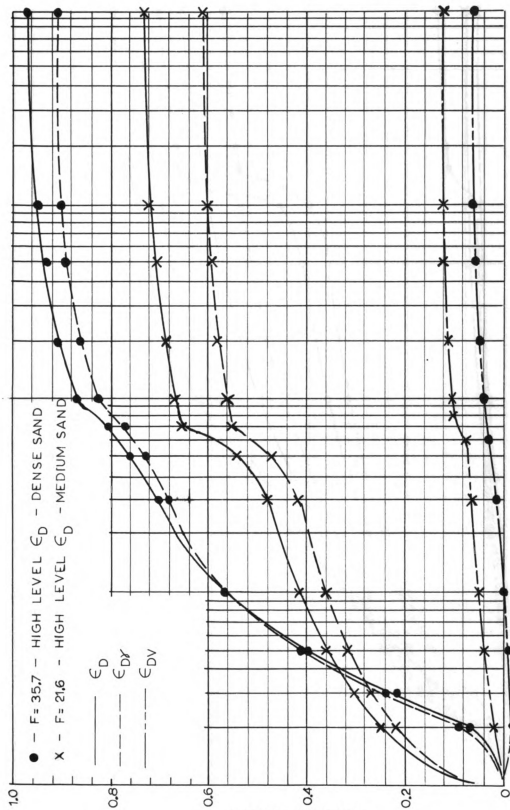

Fig. 34.-- Axial strain: shear-vs-volume deformations

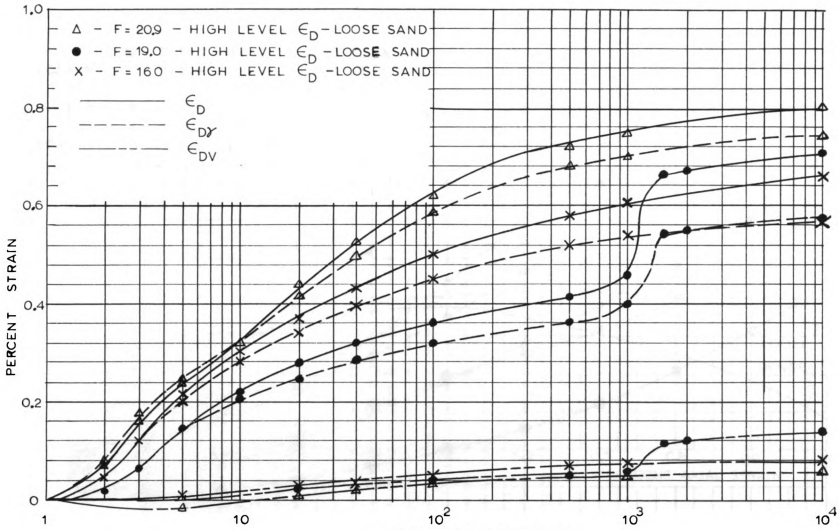

Fig. 35.--Axial strain: shear-vs-volume deformation

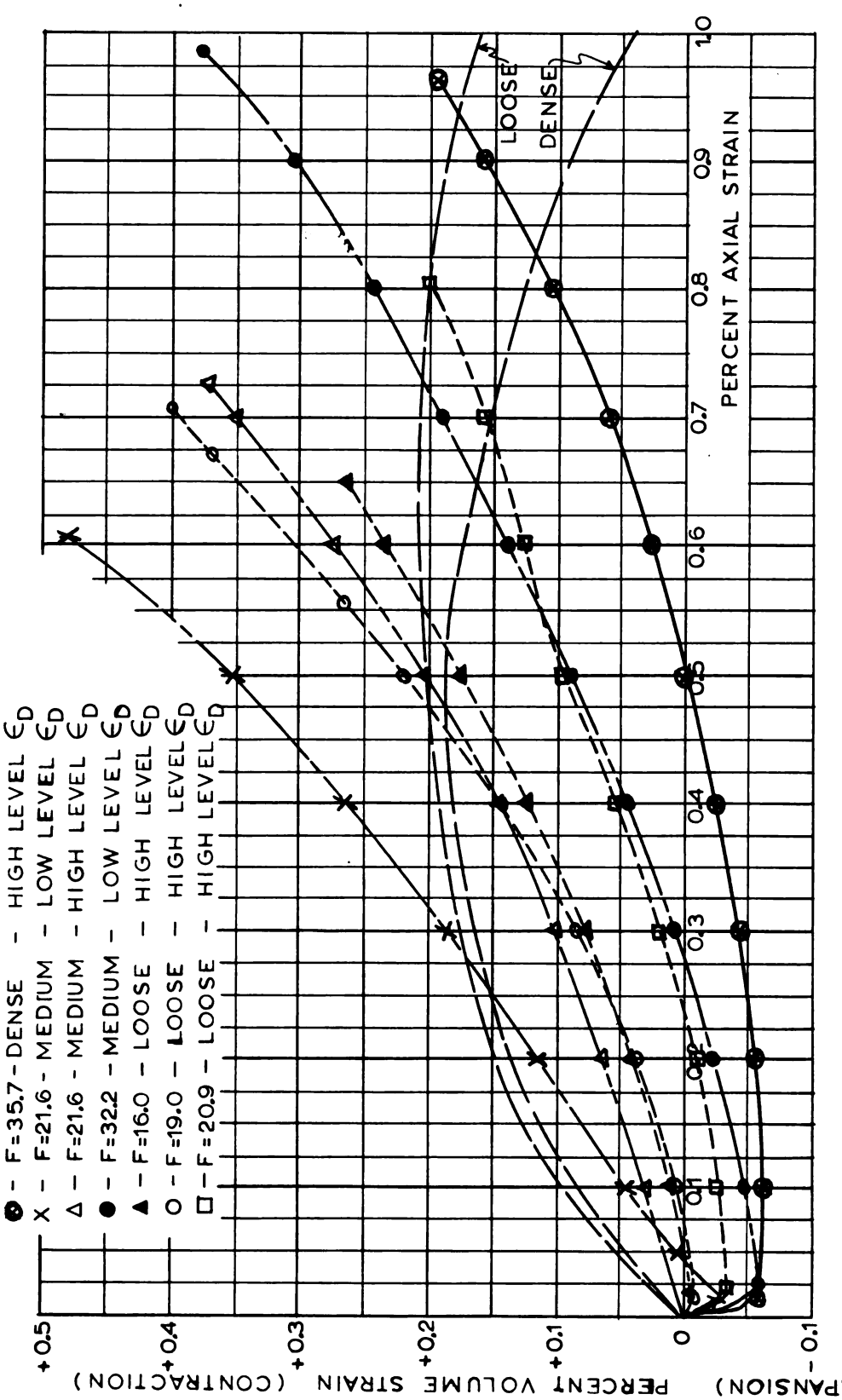

Fig. 36.--Axial -vs- volume strain

toward expansion. On the other hand, under dynamic stress, as the axial strain increased, there was a tendency toward increased densification of the sand.

From the above observations concerning Figures 33 through 36, a general statement can be made concerning the dual level strain phenomenon. Since the strain path transitions appear in the curves relating both axial strain (ϵ_D , ϵ_{DV}, and $\epsilon_{D\gamma}$) and volumetric strain to the number of stress cycles, and since the ratio of volumetric strain to axial strain remained essentially constant before, during, and after the transitions occurred, it appears that the difference between the high level and low level strains was not exclusively a result of either shear deformations or volumetric deformations. Rather, the dual strain level characteristic was a strain rate phenomenon with both types of deformation contributing proportionately at both strain levels.

3.4 Nonsymmetrical Cyclic Stress Effects

The preceding sections concern tests in which the soil was first subjected to a static stress ratio, R_S, with a cyclic stress superimposed symmetrically on the static stress. In addition to these tests, several other tests were conducted in which the cyclic axial stress was not symmetrical, i.e., $\Delta\sigma_U \neq \Delta\sigma_D$. From this data, the relative contribution to deformation of the cyclic stress increase, $\Delta\sigma_U$, and the cyclic stress decrease, $\Delta\sigma_D$, can be observed.

In analyzing these results, it was first determined whether the axial strain was a high level or low level strain. (See p. 33.) This observed strain was then compared with the data in Figure 18 for symmetrical loading. These results are shown if Figure 37 which is a plot of the ratio of the observed strain under nonsymmetrical loading, ϵ_D^{NS} , to the corresponding strain under symmetrical loading, ϵ_D^S , versus the ratio of $\Delta\sigma_U$ to $\Delta\sigma_D$. Although there is considerable scatter and only a limited amount of data, there is an obvious trend which indicates that for a given $\Delta\sigma_U$, the ratio of ϵ_D^{NS} to ϵ_D^S is inversely proportional to $\Delta\sigma_D$.

Another way to consider the implications of this is shown in Figure 38. This figure shows two typical tests. In both tests the samples were subjected to the same confining pressure, σ_C , the same static axial stress, σ_S , and both were subjected to the same cyclic stress increase, $\Delta\sigma_U$; therefore, both tests had the same stress factor, F. The dynamic strain, ϵ_D , was greater for test 2 than for test 1, although the total cyclic stress amplitude in test 2 was less than that in test 1.

It is quite probable that the parameters used in Figure 18 could be modified to take into account the effects of nonsymmetrical loading, but available data is insufficient for detailed analysis.

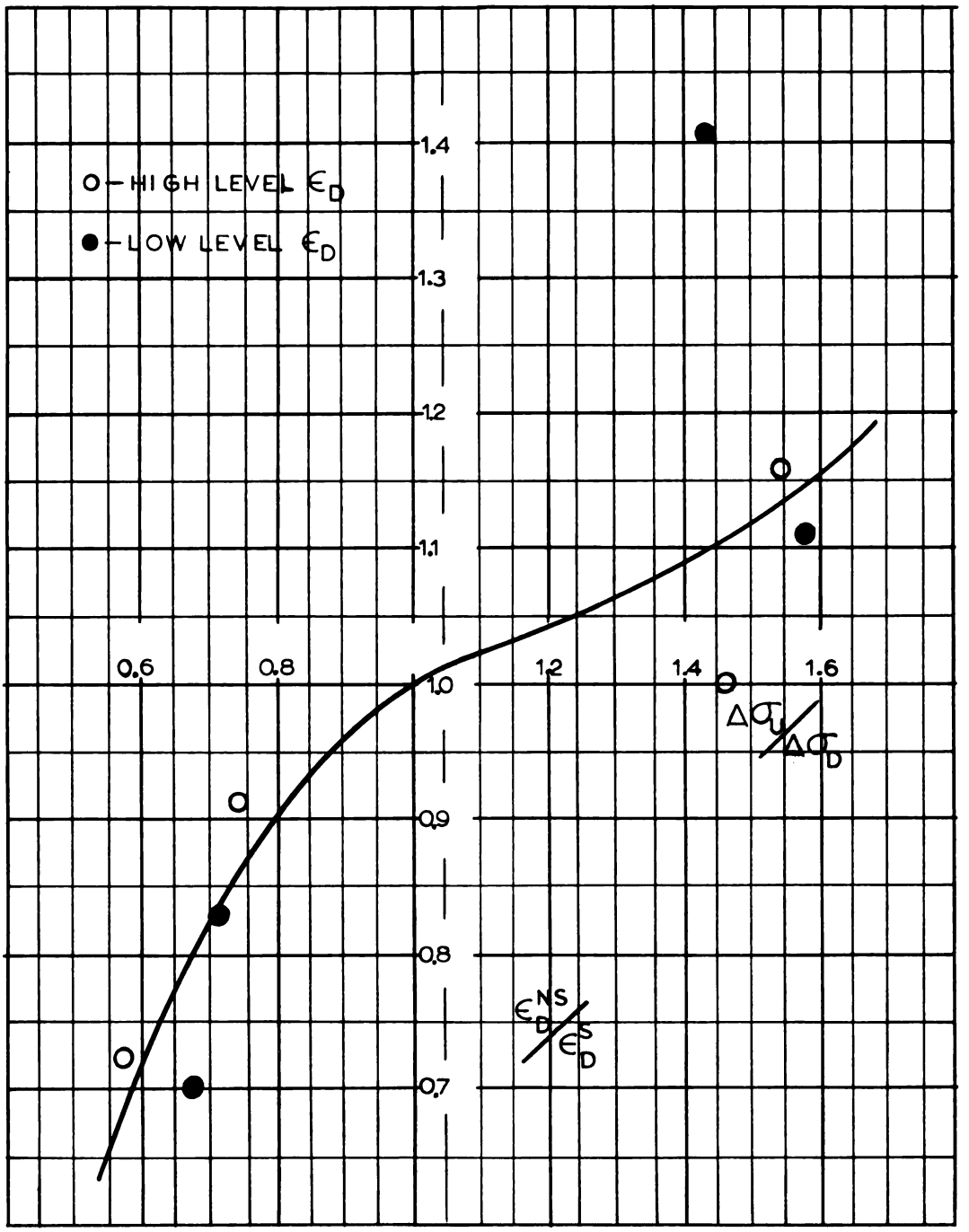

Fig. 37.--Axial strain for symmetrical -vs-nonsymmetrical cyclic loadings

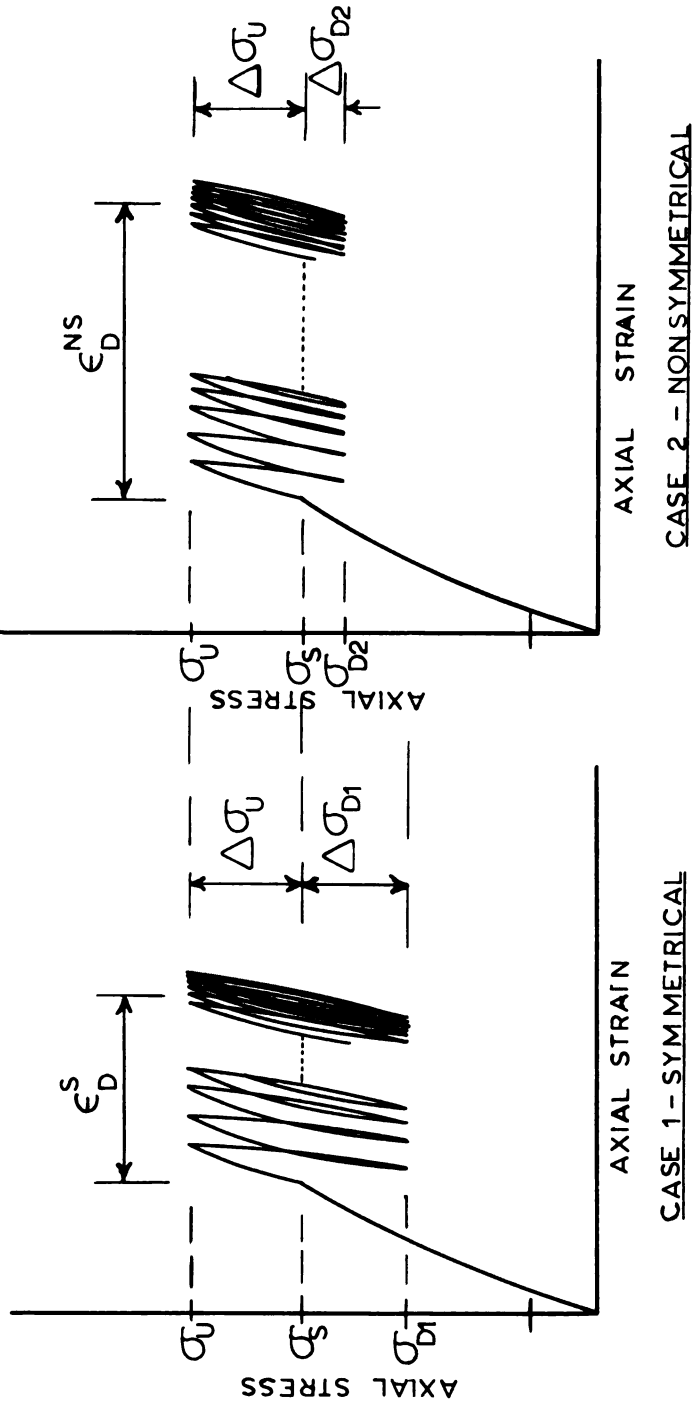

Fig. 38.--Influence of $\Delta\sigma_D$ on dynanic strain

3.5 Static Prestress Effects

In order to investigate the influence of the static stress history to which the soil is subjected, a series of tests was performed in which the soil was prestressed statically. In these tests, the specimens were first subjected to a static stress ratio of $R_p = \sigma_P / \sigma_C$. After the soil had reached equilibrium under this stress, the axial stress was reduced to a lower stress ratio of $R_s = \sigma_S / \sigma_C$. The sample was then subjected to a cyclic axial stress such that the maximum axial stress during the dynamic loading was equal to the previous prestress value, σ_P , i.e., $R_m = R_p$.

The results of these tests are plotted in Figure 39 which shows the dynamic axial strains, ϵ_D , versus the stress factor, F. This data is for sand of medium density ($e_o = .567$), and for comparison, the $F - \epsilon_D$ curves for test series A and B as plotted in Figure 18 are reproduced in this figure.

It is obvious from Figure 39 that the axial strain during the cyclic loading was considerably less for the prestressed sand. Not only was the strain less for the prestressed sand, but a specific cyclic stress amplitude had to be exceeded in order to produce any appreciable strain. This point is comparable to the F_c discussed previously. However, for the prestressed sand there was no significant strain for $F < F_c$, whereas some strain did

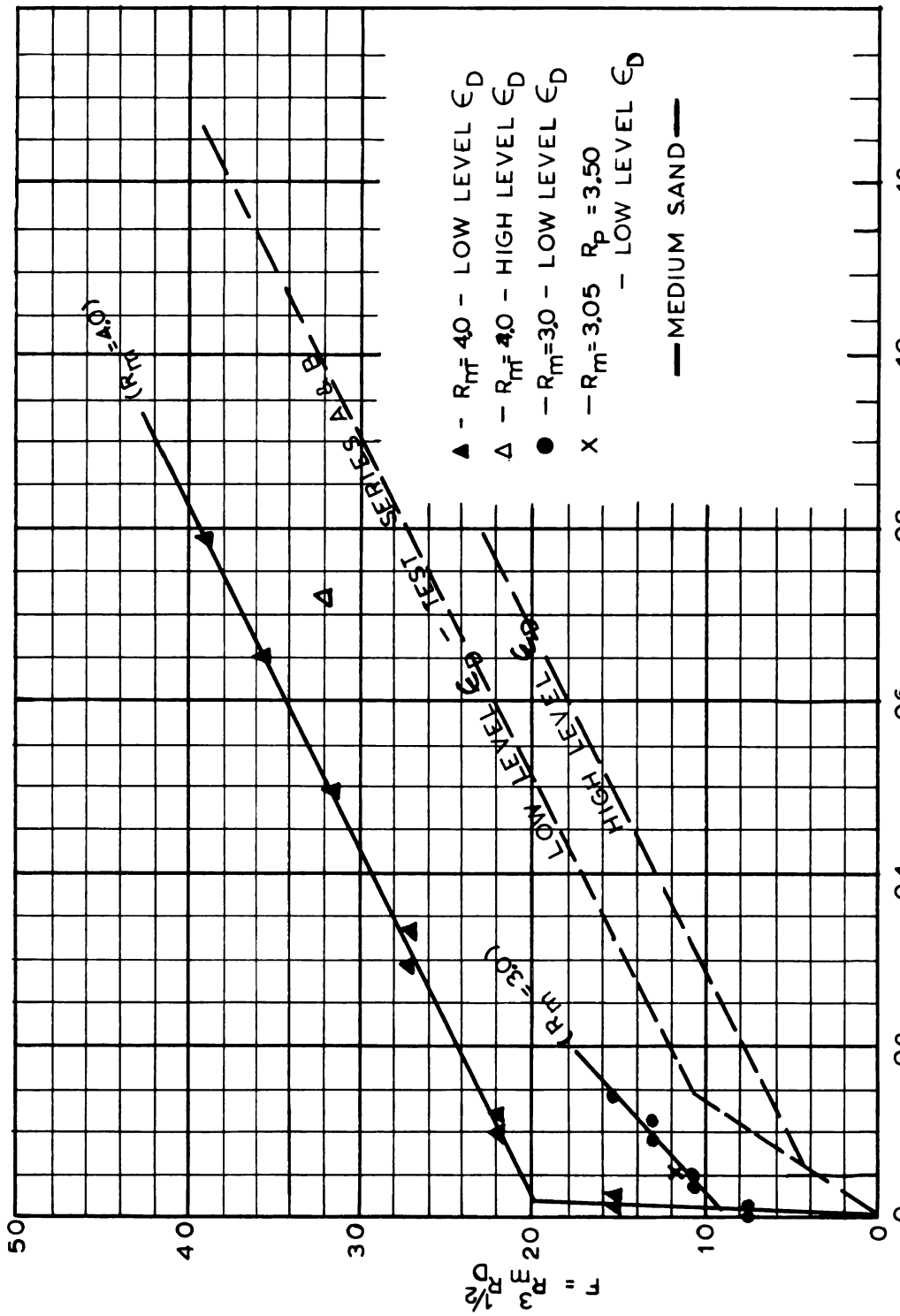

Fig. 39.--Dynamic strain-vs-stress state for prestressed sand

occur in this stress range for sand without prestressing. Also, the value of F_c for the prestressed sand was dependent upon the value of R_m whereas it was independent of R_m for sand not prestressed. For both R_m=3.0 and R_m=4.0, the value of $\Delta\sigma_U$ equals approximately 8 psi for values of F_c equal to 9 and 20 respectively. For prestressed sand, therefore, there was no significant strain as long as $\Delta\sigma_U$ was less than a specified value (8 psi in this case) which was apparently independent of the maximum stress level (providing the maximum stress level was below the failure stress level).

The axial strain for an additional test in which R_p was 15% larger than R_m is also shown in Figure 39. As can be seen, the strain was comparable to the tests with R_p=R_m.

For the prestressed sand of medium density, a high strain level was obtained in only one test. It is therefore apparent that prestressed sand had a much greater tendency toward following the lower strain path than sand which was not prestressed.

Not only was the dynamic strain less for the prestressed sand, but there was a delay of 10 to 15 stress cycles before significant strains appeared. In comparison, a high percent of the dynamic strain for soils which were not prestressed had taken place by the end of 15 stress cycles. This can be seen from curve E in Figures 12 and 14.

This characteristic could be a significant factor for a soil mass which is subjected to only a small number of stress cycles.

3.6 Cumulative Axial Strain

During the early part of the experimental testing program, a series of tests was performed in which several loading conditions were applied to the same soil specimen. (Test series E.) The dynamic strain under a given loading was considered to be the cumulative strain from that loading and previous dynamic loadings. The data from these tests are shown in Figure 40. Also shown in this figure are the F-vs-ϵ_D curves for the high level and low level strains as given in Figure 18.

The data does not divide itself into well-defined low level and high level strains; however, the magnitudes of the strain agree quite well with the data from Figure 18. One possible reason that the data do not show the two well-defined strain levels is that the control of the stresses in these tests (which were performed early in the testing program) was not up to the standards used in the main part of the testing program. Also, it is possible that one strain level could occur under one dynamic load and the other strain level occur under a subsequent loading; thus, the cumulative strain would be a mixture.

The general good agreement in strain measured in these tests and those from test series A and B indicates

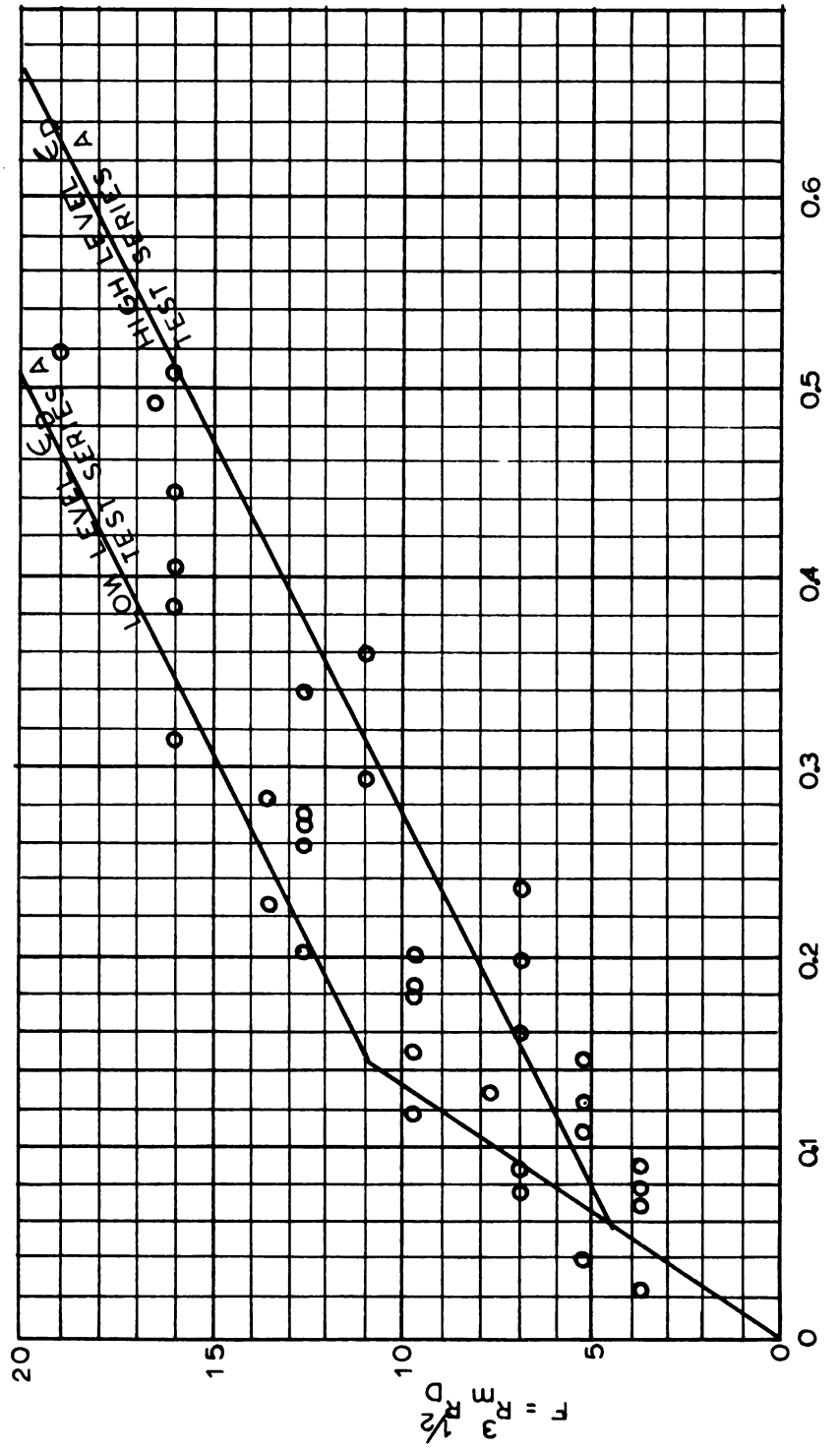

Fig. 40.--Dynamic strain-vs-stress state for cumulative loading tests

that the dynamic strain resulting from a given stress condition was independent of whether the cyclic stress was gradually built up to the given level or the full cyclic stress was applied initially.

3.7 Particle Size and Gradation Effects

A complete investigation of the influence of the soil properties on the response characteristics being discussed is beyond the scope of this project. However, tests were conducted using two other sands (test series F) primarily to determine if the high level-low level axial strain characteristic was unique to the standard Ottawa sand being used. A fine uniform Ottawa sand and a well-graded brown sand with gradations shown by curves B and C respectively in Figure 5 were used for this purpose.

The results indicate that although the magnitudes of the dynamic strains were different for the different sands, the dual strain level phenomenon occurred for all three soils.

CHAPTER IV

SUMMARY

Stress-deformation relationships under cyclic loading were obtained experimentally to develop a better understanding of soil deformation characteristics and to determine basic quantitative relationships. This was accomplished with a modified triaxial cell and a specially designed loading mechanism to apply cyclic loadings to the soil specimens.

With this apparatus, specimens of air-dried Ottawa sand were first loaded statically to a specified anisotropic stress state to represent the in situ static stresses existing under a foundation. In order to represent the loading from a vibrating foundation, a sinusoidal stress was superimposed upon the static stress state. The frequency of the cyclic loadings varied from 0.1 to 25.0 cps. The applied loads and the axial and radial deformations were measured electronically.

The variables studied were the static principal stress ratio, R_s, i.e., the ratio of axial to radial stress, the maximum stress ratio, R_m, to which the specimen was subjected during the cyclic loading, the

frequency of the cyclic loading, f, and the initial void ratio of the sand, e_o.

Variations of this testing program were also conducted in order to investigate the effects of static prestress, of progressive increases in the cyclic stress magnitude, of the nonsymmetry of the cyclic stress with respect to the static stress, and of the particle size and gradation of the soil.

The axial strain resulting from 10,000 cycles of loading was considered as the dynamic strain under the given stress condition. For a sand with a given initial void ratio, this dynamic strain was correlated with a stress factor $F=R_m^3 R_D^{\frac{1}{2}}$, where $R_D=(R_m-R_s)/R_m$. The dynamic strain for a given stress state was not unique, however. It was found to have two distinct possible magnitudes; a higher strain level and a lower strain level. The frequency of having a higher strain level increased as the initial void ratio, and the stress factor, F, increased.

Two stress levels, F_c and F_f, of practical significance were noted for the experimental data. The dynamic strains for loadings where F was smaller than F_c were small. When F was greater than F_c, the resulting dynamic strains were proportionately much larger. F_f denotes the stress level at which the sand specimen would fail under the dynamic loading. For loadings with F less than F_f, the dynamic strains were of limited, well-defined

magnitudes. For loadings with F larger than F_f, the dynamic strains were much larger and of indefinite magnitude. F_f was found to be a function of the magnitude of the cyclic stress represented by the factor R_D.

The dynamic strains were found to be independent of the frequency of the load applications for frequencies between 2.5 and 25.0 cps; however, the strains were larger for slow repetitive loadings at 0.1 cps.

The effect of static prestress was investigated by subjecting specimens to a static stress ratio of R_p and then reducing the stress ratio to a lower value, R_s, before the cyclic load was applied. The resulting dynamic strains were significantly less than those occuring for specimens which had not been prestressed.

The volumetric strains were measured during the experimental investigation and were found to be a function of R_m and R_s. For tests with R_s below a certain value, R_v, the soil densified during the cyclic loading with the amount of densification increasing as R_m increased. For tests with R_s greater than R_v, the soil expanded during the cyclic loading. The expansion increased with increasing R_m.

The dynamic axial strains were separated into two components; one due to volumetric deformation and one due to shearing deformation. It was found that a high

percentage of axial strain (75% to 95%) was due to shearing deformation.

Much of the information obtained from this study is of a qualitative nature which contributes to a better understanding of deformation characteristics of sand subjected to vibratory loadings. The experimental findings which correlate axial strain and failure conditions to the stress factor, F, are of a practical quantitative nature which can be used in analysis and design of foundations subjected to vibratory loadings. Although the relationships presented only apply to air-dry, standard Ottawa sand, similar relationships can be determined experimentally for other sands for use in analysis and design.

A first approximation of the irrecoverable foundation settlement that can be expected to occur progressively under a vibratory loading can be obtained. The stress factor, F, can be determined from the average vertical and radial static and cyclic stresses in the soil block supporting the foundation (Figure 1). The vertical strain, and hence settlement, can then be determined from the F-vs-ϵ_D relationships determined for that sand similar to those shown in Figure 18.

The F-vs-ϵ_D relationships can also be used to determine the allowable static and dynamic stress combination so that the resulting settlement would be within allowable limits or so that there would be a given factor

or safety against failure (as defined in this study). Although the dynamic strain, ϵ_D, has two possible strain levels for a given F, the higher strain level should obviously be used for design.

Since only one confining pressure (20 psi) was used for all tests in this investigation, caution must be exercised when applying the results. Although findings of a quantitative nature were obtained in this study, it is felt that the results may depend on the confining pressure. This factor should be investigated further before the foundation settlement problem can be adequately analyzed.

BIBLIOGRAPHY

1. Alpan, Issac. "Machine Foundations and Soil Resonance," Geotechnique, XI (1961), pp. 95-113.

2. Barkan, D. D. Dynamics of Bases and Foundations. New York: McGraw-Hill Book Company, 1962.

3. Bazant and Dvorak. "Effects of Vibrations on Sand and Measurement of Dynamic Properties," Proc. of Sixth International Conference on Soil Mechanics and Foundation Engineering, (1965).

4. Bernhard, R. K. "Static and Dynamic Soil Compaction," Proc. of Highway Research Board, XXXI (1952), pp. 563-592.

5. Bernhard, R. K. "Microseismics," ASTM Special Technical Publication No. 206, (1956), pp. 83-102.

6. Bernhard, R. K. "A Study of Soil Wave Propagation," Proc. of Highway Research Board, XXXVII (1958), pp. 619-646.

7. Bernhard, R. K. "On Determination of Dynamic Characteristics of Soils in Situ," ASTM Special Technical Publication No. 254, (1959), pp. 327-339.

8. Bernhard, R. K. "Biaxial Stress Fields in Non-cohesive Soils Subjected to Vibratory Loads." ASTM Special Technical Publication No. 305, (1961), pp. 3/13.

9. Bernhard, R. K., and J. Finelli. "Pilot Studies on Soil Dynamics," ASTM Special Technical Publication No. 156, (1953), pp. 211-253.

10. Bishop, Alan W., and D. J. Henkel. The Measurement of Soil Properties in the Triaxial Test. London: Edward Arnold Publishers, 1962.

11. Converse, Frederick J. "Compaction of Sand at Resonant Frequency," ASTM Special Technical Publication No. 156, (1953), pp. 124-137.

12. Corps of Engineers. "Development and Evaluation of Soil Bearing Capacity of Foundations of Structures," U. S. Army Engineer Waterways Experiment Station - Corps of Engineers - Vicksburg, Miss. Technical Report No. 3-632, Report 1, (July, 1963).

13. Drnevich, V. P., and J. R. Hall, Jr. "Transient Loading Tests on Circular Footing," Journal of Soil Mechanics and Foundations Division, Proceedings of ASCE, XCII (Nov., 1966), No. SM6, pp. 153-167.

14. Farouki, Omar T., and Hans F. Winterkorn. "Mechanical Properties of Granular Systems," Highway Research Record No. 52, (1964), pp. 10-42.

15. Goldstein, M. N., and V. Goldstein. "Contribution to the Theoretical Study of Vibrosinking of Pile Shells," Proc. of Second Asian Regional Conference of Soil Mechanics and Foundation Engineering, (1963), pp. 243-245.

16. Gomes, Lino, and Leroy Graves. "Stabilization of Beach Sand by Vibrations," Highway Research Board Bulletin 325, (1962), pp. 44-54.

17. Hall, J. R., Jr., and F. E. Richart, Jr. "Dissipation of Elastic Wave Energy in Granular Soils," Jour. of Soil Mechanics and Foundations Division, Proc. of ASCE, LXXXIX (Nov. 1963), No. SM6, pp. 27-56.

18. Hardin, B. O. "The Nature of Damping in Sands," Jour. of Soil Mechanics and Foundations Division, Proc. of ASCE, XCI, (Jan., 1965), pp. 63-97.

19. Hardin, B. O. and W. L. Black. "Sand Stiffness under Various Triaxial Stresses," Jour. of Soil Mechanics and Foundations Division, Proc. of ASCE, XCII, No. SM2, (March, 1966), pp. 27-42.

20. Haythornthwaite, R. M. "Mechanics of the Triaxial Test for Soils," Jour. of Soil Mechanics and Foundations Division, Proc. of ASCE, LXXXVI (Oct., 1960), No. SM5, pp. 35-62.

21. Johnson, Rodney W., and Eldon J. Yoder. "Pore Pressure and Strength Characteristics of Sand-Soil Mixtures under Repeated Dynamic Loads," Proc. of Second Asian Regional Conference on Soil Mechanics and Foundation Engineering, (1963), pp. 141-151.

22. Leonards, G. A., (ed.), Foundation Engineering. New York: McGraw-Hill Book Company, 1962.

23. Linger, Don A. "Effect of Vibration on Soil Properties," Highway Research Record No. 22, (1963), pp. 10-22.

24. Luscher, Ulrich, and P. Ortigosa, K. Rocker, and R. V. Whitman. "Repeated Load and Vibration Tests upon Sand," Soils Publication No. 203, Department of Civil Engineering, M.I.T. (Aug. 1967).

25. Lysmer, J. "Vertical Motion of Rigid Footings," U. S. Army Engineer Waterways Experiment Station-Corps of Engineers - Vicksburg, Miss. - Contract Report No. 3-115, (June, 1965).

26. Lysmer, J., and F. E. Richart, Jr. "Dynamic Response of Footings to Vertical Loading," Jour. of Soil Mechanics and Foundations Division, Proc. of ASCE, XCII (Jan., 1966), pp. 65-91

27. Mogami, T. "The Behavior of Soil During Vibration," Proc. of Third International Conference of Soil Mechanics and Foundation Engineering, Vol. 1, (1953), pp. 152-155.

28. Murphy, V. A. "The Effect of Ground Characteristics on the Aseismic Design of Structures," Proc. of Second World Conference on Earthquake Engineering, Vol. 1, (1960), pp. 231-247.

29. Okamoto, Shunzo, and Katsuyuki Seimiya. "An Experimental Study on Settlement of Foundation Due to Vibration," Proc. of Fourth Japan National Congress for Applied Mechanics, (1954), pp. 109-110.

30. Richart, F. E., Jr. "Foundation Vibrations," Transactions of ASCE, CXXVII, Part 1, (1962), pp. 863-925.

31. Richart, F. E., Jr., J. R. Hall, and Y. S. Chae. "Dynamic Pressure Distribution beneath a Vibrating Footing," Proc. of Sixth International Conference on Soil Mechanics and Foundation Engineering, Vol. 2, (1965), pp. 22-26.

32. Richart, F. E., Jr., and R. V. Whitman. "Comparison of Footing Vibration Tests with Theory," Jour. of Soil Mechanics and Foundations Division, Proc. of ASCE, XCIII, No. SM6, (Nov. 1967), pp. 143-168.

33. Seed, H. Bolton. "A Method for Earthquake Resistant Design of Earth Dams," Jour. of Soil Mechanics and Foundations Division, Proc. of ASCE, XCII, No. SM1, (Jan., 1966), pp. 13-41.

34. Seed, H. Bolton, and Richard E. Goodman. "Earthquake Stability of Slopes of Cohesionless Soils," Jour. of Soil Mechanics and Foundations Division, Proc. of ASCE, XC, No. SM6, (Nov., 1964), pp. 43-73.

35. Seed, H. Bolton, and J. W. N. Fead. "Apparatus for Repeated Load Tests on Soils," ASTM Special Publication No. 254, (1959), pp. 78-87.

36. Seed, H. Bolton, and K. L. Lee, "Liquefaction of Saturated Sands during Cyclic Loading," Jour. of Soil Mechanics and Foundations Division, Proc. of ASCE, XCII, No. SM6, (Nov., 1966), pp. 105-134.

37. Seed, H. Bolton, and K. L. Lee. "Cyclic Stress Conditions Causing Liquification of Sand," Jour. of Soil Mechanics and Foundations Division, Proc. of ASCE, XCIII, No. SM1, (Jan., 1967), pp. 47-70.

38. Seed, H. Bolton, and K. L. Lee. "Dynamic Strength of Anisotropically Consolidated Sand," Jour. of Soil Mechanics and Foundations Division, Proc. of ASCE, CXIII, No. SM5, (Sept., 1967), pp. 169-190.

39. Sung, Tse Yung. "Vibrations in Semi-Infinite Solids Due to Periodic Surface Loading," ASTM Special Technical Publication No. 156, (1953), pp. 35-63.

40. Tanimoto, Kiichi. "A Method of Estimating the Degree of Compaction of Sandy Soils," Soil and Foundation, Vol. 5, No. 1, (Dec., 1964).

41. Tschebotarioff, Gregory P. "Effect of Vibrations on the Bearing Properties of Soils," Proc. of Highway Research Board, XXIV (1944), pp. 404-423.

42. Tschebotarioff, Gregory P., and George W. McAlpin. "Vibratory and Slow Repetitional Loading of Soils," Proc. of Highway Research Board, XXVI (1946), pp. 551-561.

43. Wallace, William L. "Displacement of Long Footings by Dynamic Loads," Jour. of Soil Mechanics and Foundations Division, Proc. of ASCE, LVII, No. SM5 (Oct., 1961), pp. 45-68.

44. Watanabe, Takashi. "Compaction of Sandy Ground by Vibration - Vibroflotation and Related Problems," Proc. of Second Asian Regional Conference on Soil Mechanics and Foundation Engineering, Vol. 1, (1963), pp. 406-410.

45. Weissmann, G. F., and R. R. Hart. "The Damping Capacity of some Granular Soils," ASTM Special Technical Publication No. 305, (1961), pp. 45-54.

46. Whitman, Robert V., and Kent A. Healy. "Shear Strength of Sands During Rapid Loadings," Transactions of ASCE, CXXVIII, Part I, (1963), pp. 1553-1586.

47. Winterkorn, Hans F. "Macromeritic Liquids," ASTM Special Technical Publication No. 156, (1953), pp. 77-89.

APPENDIX A

VOLUMETRIC STRAIN MEASUREMENTS

The volumetric strain determinations for this investigation were obtained by two methods. First, the volume change was determined by measuring the amount of air forced in or out of the sample by the method described in Chapter II. The second method consisted of calculating the volume change from the radial deformation at the mid-height of the sample and the axial deformation.

Since the volume change measuring system had to be operated manually, the volume fluctuations during one stress cycle could not be measured by the first method. The accumulated volume change after a given number of cycles could, however, be determined by this method. The main problem with this method was the influence of room and sample temperature on the measurements.

In order to properly account for this influence, several samples were prepared and the measured volume change was then plotted as a function of the room temperature change. During this time period, the electronic measurements of the axial and radial deformations of the

sample were monitored to insure that the sample was not actually deforming. The data thus obtained are shown in Figure 41. There was some scatter in the data, particularly for larger changes in temperature. However, since the temperature change which occurred during a test was always less than 1.0 °C., a volumetric reading reduction of 0.20 cm^3 per 1.0 °C. increase in room temperature was considered satisfactory for the temperature correction.

Since the measurement of displaced air was sensitive to temperature changes, the question of possible heat generation within the soil sample arose. To investigate this possibility, a thermocouple was inserted into the center of several sand specimens and the temperature changes were monitored during the progress of the tests. The measuring system had an accuracy of 0.5 °C. which would indicate whether heat was being generated during the cyclic loading to affect the volume change measurements. At no time during this series of tests were there any temperature changes which could be attributed to heat generation within the sample.

In the second method of measuring volumetric strain, it was possible to determine the volumetric strain at any given time or for any increment of time. The main problem with this method was that the radial sample deformation was only measured at mid-height, and therefore, any non-uniform sample deformations would affect

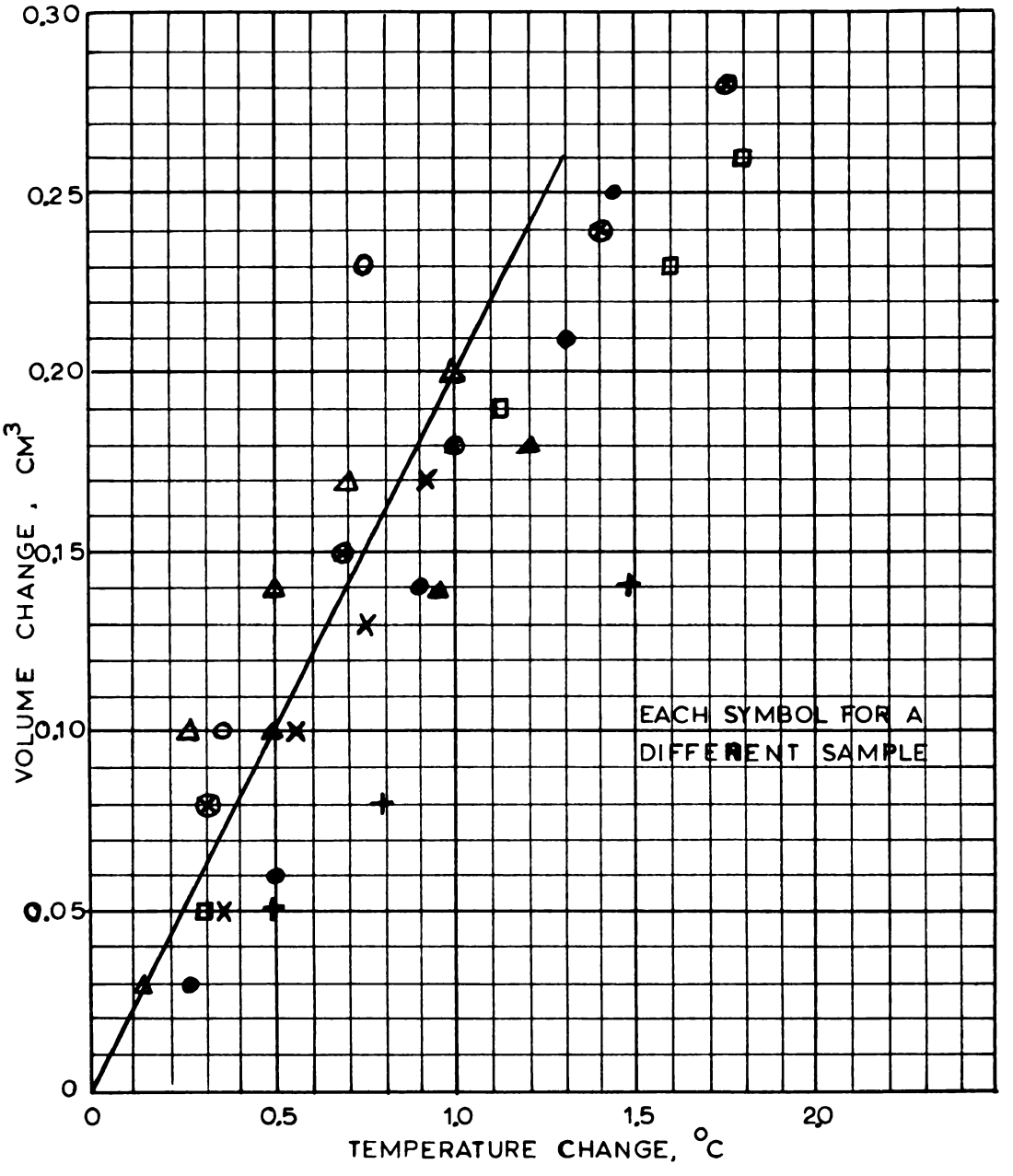

Fig. 41.--Apparent volume change -vs- temperature change

the results.

Due to end restraints, the radial deformations at the ends of the sample were less than at the center where the measurements were taken. Therefore, the measured radial deformation was greater than the average radial deformation of the sample. Upon comparison of the volumetric strains determined by the two methods, it was observed that if the average radial strain of the sample was taken as $\frac{1}{2}$ the measured strain at the mid-height, the volumetric strain determinations by the two methods were, for all practical considerations, in consistent agreement. A plot comparing the volume changes determined by the two methods is given in Figure 42. This criteria was used in calculating volumetric strains throughout the testing program.

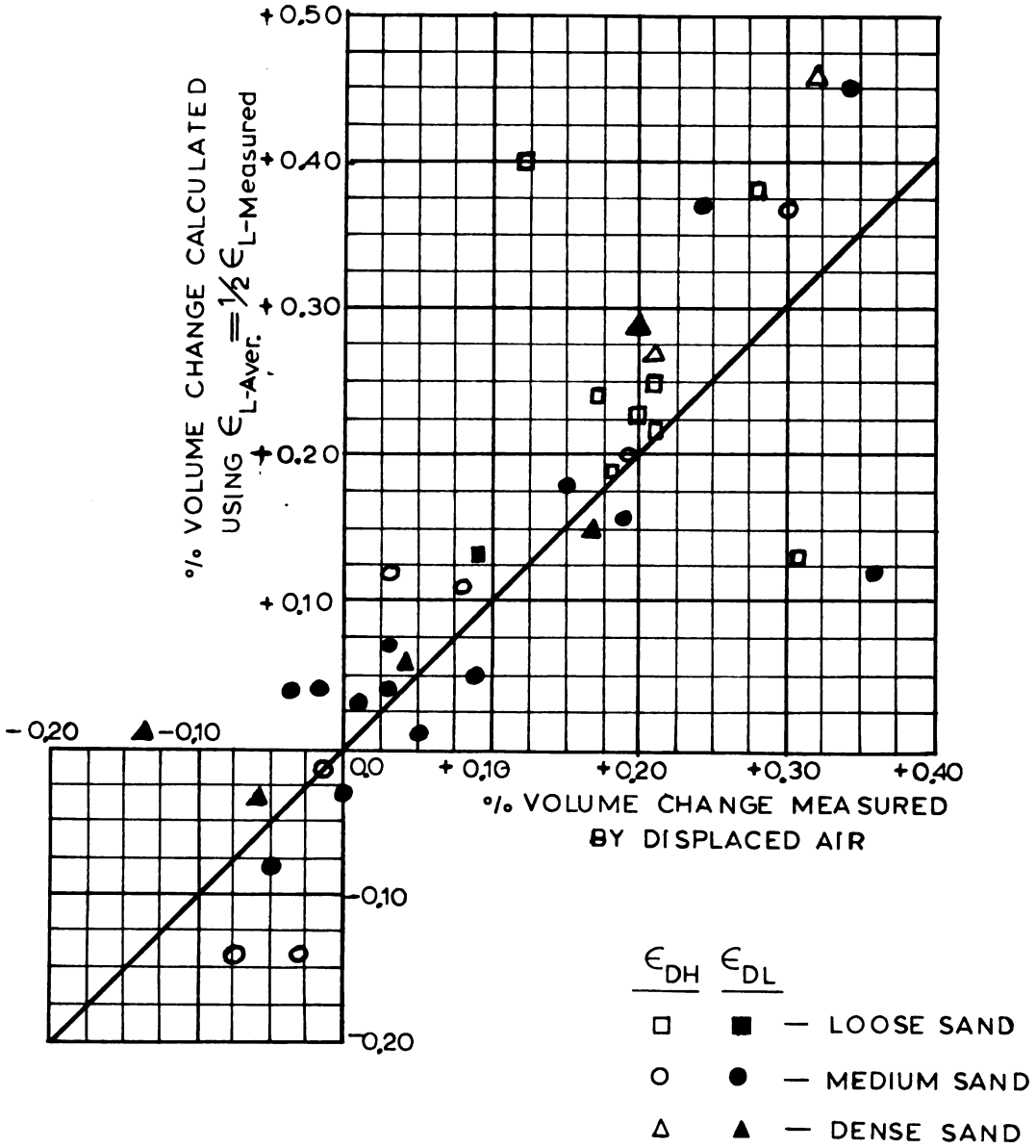

Fig. 42.--Calculated -vs-measured volume changes

APPENDIX B

SUMMARY OF TEST DATA

Tables I through VIII summarize the test variables and results of the individual specimens.

Table I Summary of data for tests with loose sand

Test No.	e_o	f (cps)	R_s	R_m	R_D	F	ϵ *	ϵ_{vol} Calc.	ϵ_{vol} Meas.
67-R	.615	10	2.25	2.90	.224	11.4	0.29 L	0.13	0.09
58	.605	10	2.50	3.425	.270	20.9	0.81 H	0.19	0.18
65-R	.620	10	2.50	3.225	.225	16.0	0.65 H	0.25	0.21
66-R	.618	10	2.25	3.10	.274	15.6	0.62 H	0.38	0.28
61-RS	.599	10	2.50	3.35	.254	19.0	0.71 H	0.40	0.12
77-R	.605	5	1.75	2.15	.186	4.3	0.23 H	0.23	0.20
78-R	.607	5	2.50	3.00	.167	11.0	0.43 H	0.24	0.17
79-R	.605	2.5	2.00	2.275	.121	4.1	0.16 H	0.13	0.31
86-R	.603	10	2.00	2.65	.245	9.2	0.39 H	0.22	0.21
57	.599	10	2.50	3.75	.333	30.6	1.45 F		
67-R	.615	10	3.50	3.90	.102	19.0	2.11 F		
79-R	.605	2.5	2.75	3.175	.134	11.7	0.81 F		
85-R	.603	5	2.75	3.45	.203	18.5	1.67 F		

* L - Low Level Axial Strain
H - High Level Axial Strain
F - Failure Occured

Table II Summary of data for tests with medium sand

Test No.	e_o	f (cps)	R_s	R_m	R_D	F*	ϵ_D*	ϵ_{vol} Calc.	ϵ_{vol} Meas.
42	.560	10	2.25	3.35	.328	21.6	0.60 L	0.45	0.34
45	.570	10	2.50	3.40	.265	20.2	0.53 L	0.18	0.15
46	.560	10	1.75	2.15	.186	4.3	0.06 L	0.05	0.09
46-2	.560	10	2.50	3.80	.342	32.2	0.96 L	0.37	0.24
47	.575	10	1.75	2.425	.278	7.6	0.11 L	0.04	-0.02
50	.575	2.5	3.50	3.80	.079	15.4	0.31 L	-0.08	-0.05
52	.566	2.5	2.00	2.80	.285	11.7	0.18 L	0.12	0.36
52-2	.566	2.5	3.00	4.25	.294	41.7	1.34 L		-0.07
56	.570	5	2.50	3.20	.219	15.3	0.32 L	0.16	0.19
44	.566	10	1.50	2.05	.268	4.5	0.07 L	0.08	
63-R	.575	10	3.25	3.55	.084	13.0	0.19 L	0.01	0.05
48-F	.566	10	2.50	3.50	.285	23.0	0.77 H		0.19
41	.560	10	2.25	2.825	.203	10.2	0.29 H	0.20	0.19
54	.567	2.5	2.50	3.45	.275	21.6	0.73 H	0.37	0.30
60-R	.575	10	2.50	3.325	.248	18.4	0.61 H	0.11	0.08
92-R	.560	5	2.50	3.78	.339	31.5	1.13 H	0.45	
95-R	.560	25	2.50	2.90	.138	9.0	0.27 H	0.12	0.03
51	.581	2.5	3.25	3.85	.156	22.6	0.92 F		
83-RSP	.560	0.1	2.50	3.25	.230	16.5	0.64 H	0.11	
84-RSP	.566	0.1	2.50	3.00	.166	11.0	0.23 L	0.04	
96-R1	.564	6	2.00	2.18	.082	3.0 P	0.04 L	0.03	0.01
96-R2	.564	6	2.00	2.25	.111	3.8 P	0.05 L	0.04	0.03
96-R3	.564	6	3.00	3.50	.143	16.2 P	0.52 H	0.04	-0.04
97-R1	.566	6	2.50	2.82	.113	7.6 P	0.09 L	0.03	0.01
97-R2	.566	6	3.50	3.79	.076	15.1 P	0.44 H	-0.08	-0.14
98-R1	.570	6	2.00	2.25	.111	3.8 P	0.05 L	0.03	0.07
98-R2	.570	6	3.00	3.17	.053	7.4 P	0.11 L	-0.03	0.00
98-R3	.570	6	3.00	3.49	.140	16.0 P	0.51 H	-0.14	-0.03

* L - Low Level Axial Strain
  H - High Level Axial Strain
  F - Failure Occured
  P - Pulsation Confining Pressure

Table III Summary of data for tests with dense sand

Test No.	e_o	f (cps)	R_s	R_m	R_D	F	ϵ_D *	ϵ_{vol} Calc.	ϵ_{vol} Meas.
62-RS	.540	10	2.50	3.325	.248	18.3	0.23 L	0.15	0.17
68-R	.534	10	2.25	2.90	.224	11.5	0.15 L	0.06	0.04
68-R2	.534	10	3.25	3.825	.150	21.7	0.34 L	0.01	-0.14
75-R	.535	10	3.25	3.975	.182	26.9	0.53 L	-0.03	-0.06
90-R	.521	5	2.50	3.75	.333	30.5	0.67 L	0.29	0.20
73-R	.535	10	3.00	4.10	.268	35.7	0.96 H	0.19	-0.11
88-R	.530	5	2.50	3.95	.367	37.5	1.07 H	0.46	0.32
91-R	.539	5	2.50	3.50	.286	23.0	0.53 H	0.27	0.21
74-R	.536	10	3.25	4.025	.193	28.6	1.04 F		
76-R	.531	10	3.25	4.10	.207	31.4	1.24 F		
87-R	.528	5	3.25	4.30	.244	39.3	2.72 F		

* L - Low Level Axial Strain
H - High Level Axial Strain
F - Failure Occured

Table IV Summary of data from tests with a non-symmetrical axial pulse

Test No.	e_o	f (cps)	R_s	R_m	R_n	R_D	F	ϵ_D^{NS*}	ϵ_D^S	$\epsilon_D^{NS}/\epsilon_D^S$	$\frac{\Delta\sigma_u}{\Delta\sigma_D}$
38	.575	10	2.50	3.35	1.95	.254	19.0	0.74 H	0.64	1.16	1.55
40	.575	10	2.50	3.15	2.05	.206	14.2	0.41 L	0.29	1.41	1.44
47	.575	10	3.00	3.30	2.60	.091	10.8	0.30 H	0.33	0.91	0.75
45	.570	10	1.75	2.225	1.425	.213	5.1	0.09 H	0.09	1.00	1.46
64-R	.560	10	3.00	3.675	2.575	.184	21.2	0.62 L	0.56	1.11	1.59
50	.575	2.5	2.50	2.80	2.05	.107	7.2	0.07 L	0.10	0.70	0.67
51	.581	2.5	2.50	2.75	2.05	.091	6.3	0.11 H	0.15	0.73	0.56
85-R	.603	10	2.00	2.25	1.65	.111	3.8	0.05 L	0.06	0.83	0.71

* L - Low Level Axial Strain
  H - High Level Axial Strain

Table V Summary of data for prestressed medium sand

Test No.	e_o	f	R_s	R_p	R_m	R_D	F	ϵ_D^*
18-1	.563	10	2.75	3.00	3.00	.083	7.8	0.01 L
18-2	.563	10	2.50	3.00	3.00	.167	11.0	0.04 L
18-3	.563	10	2.25	3.00	3.00	.250	13.5	0.09 L
18-4	.563	10	2.00	3.00	3.00	.333	15.6	0.14 L
19-1	.570	10	2.75	3.00	3.00	.083	7.8	0.00 L
19-2	.570	10	2.50	3.00	3.00	.167	11.0	0.04 L
19-3	.570	10	2.25	3.00	3.00	.250	13.5	0.11 L
18-5	.563	10	3.75	4.00	4.00	.063	16.0	0.02 L
18-6	.563	10	3.50	4.00	4.00	.125	22.6	0.13 L
18-7	.563	10	3.25	4.00	4.00	.187	27.7	0.30 L
18-8	.563	10	3.00	4.00	4.00	.250	32.0	0.50 L
18-9	.563	10	2.75	4.00	4.00	.313	35.8	0.65 L
18-10	.563	10	2.50	4.00	4.00	.375	39.2	0.79 L
19-4	.570	10	3.75	4.00	4.00	.063	16.0	0.01 L
19-5	.570	10	3.50	4.00	4.00	.125	22.6	0.10 L
19-6	.570	10	3.25	4.00	4.00	.187	27.7	0.33 L
19-7	.570	10	3.00	4.00	4.00	.250	32.0	0.72 H
82-RU	.568	10	2.50	3.50	3.05	.180	12.0	0.05 L

* L - Low Level Axial Strain
  H - High Level Axial Strain

Table VI Summary of data from cumulative loading tests on medium sand

Test No.	e_o	f (cps)	R_s	R_m	R_D	F	ϵ_D
13-1	.555	7.5	2.00	2.25	.111	3.8	0.09
13-2	.555	7.5	2.00	2.375	.158	5.3	0.14
13-3	.555	7.5	2.00	2.50	.200	7.0	0.20
14b-1	.585	10	2.00	2.25	.111	3.8	0.02
14b-2	.585	10	2.00	2.375	.158	5.3	0.04
14b-3	.585	10	2.00	2.50	.200	7.0	0.08
15-1	.555	15	2.00	2.25	.111	3.8	0.08
15-2	.555	15	2.00	2.375	.158	5.3	0.11
15-3	.555	15	2.00	2.50	.200	7.0	0.17
14a-1	.570	10	2.00	2.25	.111	3.8	0.07
14a-2	.570	10	2.00	2.375	.158	5.3	0.12
27	.559	10	2.00	2.50	.200	7.0	0.10
13-4	.555	7.5	3.00	3.25	.077	9.5	0.13
13-5	.555	7.5	3.00	3.375	.111	12.7	0.27
13-6	.555	7.5	3.00	3.50	.143	16.2	0.50
14-1	.568	10	3.00	3.25	.077	9.5	0.20
14-2	.568	10	3.00	3.375	.111	12.7	0.33
14-3	.568	10	3.00	3.50	.143	16.2	0.51
14a-4	.570	10	3.00	3.25	.077	9.5	0.16
14a-5	.570	10	3.00	3.375	.111	12.7	0.27
14a-6	.570	10	3.00	3.50	.143	16.2	0.42
15-4	.555	15	3.00	3.25	.077	9.5	0.18
15-5	.555	15	3.00	3.375	.111	12.7	0.27
15-6	.555	15	3.00	3.50	.143	16.2	0.38
28	.579	10	2.50	3.00	.167	11.0	0.29
31	.577	10	2.25	3.00	.250	13.5	0.28
31a	.581	10	2.25	3.00	.250	13.5	0.23
28a	.581	10	2.50	3.00	.167	11.0	0.36
36	.581	10	2.75	3.00	.083	7.9	0.13
31a-2	.581	10	2.25	3.25	.308	19.0	0.52

Table **VII** Summary of data for fine Ottawa sand

Test No.	e_o	f (cps)	R_s	R_m	R_D	F	ϵ_D^*
70-RF	.719	10	2.50	3.525	.290	23.8	1.32 L
71-RF	.678	10	2.50	3.00	.167	11.0	0.32 L
72-RF	.680	10	2.50	3.25	.230	16.7	1.02 H

* L - Low Level Axial Strain
  H - High Level Axial Strain

Table VIII Summary of data for well-graded brown sand

Test No.	e_o	f (cps)	R_s	R_m	R_D	F	ϵ_D^*
93-R	.635	10	2.50	3.50	.285	23.0	0.63 L
94-R	.638	10	2.50	3.425	.270	20.9	0.67 H

* L - Low Level Axial Strain
  H - High Level Axial Strain